

See discussions, stats, and author profiles for this publication at: <https://www.researchgate.net/publication/358328715>

Fuzzy subspace clustering noisy image segmentation algorithm with adaptive local variance & non-local information and mean membership linking

Article in *Engineering Applications of Artificial Intelligence* · April 2022

DOI: 10.1016/j.engappai.2022.104672

CITATIONS

4

READS

66

4 authors, including:



Tongyi Wei

Lanzhou Jiaotong University

1 PUBLICATION 4 CITATIONS

[SEE PROFILE](#)



Fuzzy subspace clustering noisy image segmentation algorithm with adaptive local variance & non-local information and mean membership linking[☆]

Tongyi Wei, Xiaopeng Wang*, Xinna Li, Shengyang Zhu

School of Electronic and Information Engineering, Lanzhou Jiaotong University, Lanzhou 730070, China



ARTICLE INFO

Keywords:

Fuzzy subspace clustering
Noise image segmentation
Mean membership linking
Robustness

ABSTRACT

The Fuzzy C-means (FCM) clustering algorithm is an effective method for image segmentation. Non-local spatial information considers more redundant information of the image thus is more robust to noise. However, under-segmentation of non-local spatial information may exist with higher noise density. The number of iteration steps is also significant in FCM, and employing membership linking can effectively reduce the number of iteration steps. Nonetheless, when there are outliers in the membership degree, the membership linking can make the algorithm converge prematurely before reaching the optimum, affecting segmentation performance. This paper presents a fuzzy subspace clustering noisy image segmentation algorithm with adaptive local variance & non-local information and mean membership linking (FSC_LNML). Firstly, local variance templates are utilized to eliminate the under-segmentation of non-local information, and local variance & non-local information are integrated into the FCM objective function to improve robustness. Secondly, the mean membership linking is employed as the denominator of the objective function to reduce the number of iterations and solve the problem that the algorithm converges early before reaching the optimum when the membership has an outlier. Thirdly, the absolute intensity difference between the original image and the local variance & non-local information and its inverse are used to adaptively constrain the original image and the local variance & non-local information. Finally, the concept of the subspace is introduced to adaptively assign appropriate weights to each dimension of the image to improve the segmentation performance of color images. The simulation results on noisy grayscale images and noisy color images show that the efficiency of the proposed method FSC_LNML is better than other fuzzy-based clustering algorithms. The convergence proof of the algorithm is also presented.

1. Introduction

Image segmentation is one of the most important research topics in computer vision and image understanding. In the past decades, many image segmentation algorithms have been developed (Wei et al., 2021; Weng and Dong, 2021; Wang and Tu, 2012; Pont-Tuset et al., 2016; Li et al., 2006) and applied to resource surveying (Lin et al., 2021), artificial intelligence (Sodjinou et al., 2021), remote sensing data analysis (He et al., 2021), disease diagnosis (Feng et al., 2020), and other fields (Jiang et al., 2021). There are two roughly defined categories of image segmentation: supervised and unsupervised image segmentation. Unsupervised image segmentation includes clustering (Zeng et al., 2017), Graph Cut (Ma et al., 2016), watershed transformation (WT) (Bai and Urtasun, 2017), fuzzy entropy (Yin et al., 2017), etc., which are widely utilized owing to their simplicity and the nonrequirement of training samples and labels. In contrast to unsupervised algorithms,

some supervised algorithms, such as convolutional neural networks (CNN) (Krizhevsky et al., 2012) and fully convolutional networks (FCN) (Long et al., 2015), allow image segmentation by feature learning, yet they involve a large number of training samples. The clustering algorithm is a typical unsupervised image segmentation algorithm due to its simplicity, few input parameters, and good robustness. The fuzzy clustering algorithm (Han and Shi, 2007) introduces the fuzziness of image pixel attribution and is widely applied in clustering methods, where FCM (Peizhuang, 1983) is one of the most commonly employed fuzzy clustering algorithms.

In the virtual environment, images are susceptible to noise interference during acquisition and conversion due to noise uncertainty. Conventional FCM fails to consider image structural features and lacks noise suppression capability. Thus, numerous FCM variants have been presented to improve the robustness. The most popular solution is to incorporate local information into the FCM objective function. The

[☆] Code package is available in https://github.com/Jackywei1/FSC_LNML-Algorithm.

* Corresponding author.

E-mail addresses: 11200715@stu.lzjtu.edu.cn (T. Wei), wangxiaopeng@mail.lzjtu.cn (X. Wang), 13884591830@163.com (X. Li), wty19961005@gmail.com (S. Zhu).

local knowledge was introduced by the FCM_S (Ahmed et al., 2002) for the first time. Then, the algorithms of FCM_S1/S2 (Chen and Zhang, 2004), FGFCM (Cai et al., 2007), FLICM (Krinidis and Chatzis, 2010), NWFCM (Zaixin et al., 2014), NDFCM (Guo et al., 2016), Memon's method (Memon and Lee, 2018) and KWFLICM (Gong et al., 2012) successively introduced local space information to improve robustness. Although the above algorithms improve the robustness, they employ a fixed size and shape of the neighborhood search window while computing the local information. The search window corresponding to different images should be other. It is unreasonable to take a constant to set the value of the window. Consequently, it is essential to calculate the search window values adaptively. Liu's method (Liu et al., 2015a), Bai's method (Bai et al., 2015) and ADFLICM (Zhang et al., 2017) replace the fixed size and shape windows with adaptive neighborhood information, and the segmentation performance is significantly improved. The introduction of local information enhances the robustness of the FCM algorithm to some extent. Simultaneously, the local information-based FCM variant algorithm needs to calculate the distance from each pixel to the cluster center during each iteration, increasing computational complexity. Since the number of gray levels of an image is much smaller than the number of pixel levels, histogram-based FCM variants of algorithms have been proposed, such as EnFCM (Szilagyi et al., 2003), FGFCM (Cai et al., 2007), FFCM_SNLS (Zhao, 2013), FRFCM (Lei et al., 2018a) and SFFCM (Lei et al., 2018b). The image histogram consists of only grayscale values, which are much smaller than the number of pixels in the image, making clustering much faster.

The improved FCM variant considers the neighborhood information of images and utilizes histograms to speed up the clustering while neglecting the neighborhood information about membership. Hidden Markov Random Field (HMRF) (Ghamisi et al., 2013; Zhao et al., 2017; Liu et al., 2015b) can describe the relationship between pixels. Consequently, based on HMRF, Liu's method (Liu et al., 2015a), HMRF-FCM (Chatzis and Varvarigou, 2008), and FLDNICM (Zhang et al., 2018) methods are proposed. Since HMRF considers the previous state of the current membership degree and can extract the spatial context information provided by local pixel blocks, it obtains better results than FCM in image segmentation. However, the noise can destroy the contextual knowledge of the image, and the local pixel block may contain too many noisy pixels, resulting in a reduced sensitivity of the segmentation of noisy images. Meanwhile, it is difficult to obtain better classification results for nonlinear classification problems utilizing the traditional Euclidean distance. The kernel method is employed to map the data into a high-dimensional space to solve the problem that conventional Euclidean distance is sensitive to nonlinear data. Based on the kernel method, KWFLICM (Gong et al., 2012), ARKFCM (Elazab et al., 2015), GKWFLICM (Memon and Lee, 2018), and KBFWCM (Zhang et al., 2019) are proposed. Even though the kernel method can handle the nonlinear classification problem well, it is challenging to solve strong noise image segmentation due to the high uncertainty.

The adjacent pixels surrounding the central pixel may be noisy as the noise density increases, and thus it is not enough to consider only local information. It would be more sensible for the central pixel to consider blocks of pixels other than the local pixel block. Several pixels with similar neighborhood configurations are available (Buades et al., 2008). Compared with using neighboring pixels, it is more sensible to obtain the spatial information of a given pixel using pixels with similar neighborhood configurations, called non-local spatial information. Based on non-local information, FCM_NLS (Zhao et al., 2011), FCM_SNLS (Zhao, 2013), and NWFCM (Zaixin et al., 2014) are proposed. Although non-local spatial information allows for image redundancy and preserving the actual content, under-segmentation may appear due to high noise density. In addition, it assigns the same weights to the different dimensions of each pixel, indicating that each dimension of the data is treated equally. Nevertheless, the influence

of pixels between different dimensions may not be equal in clustering. Assigning appropriate weights to each dimension may enhance the performance of color image segmentation. Therefore, the concept of the subspace is proposed. Based on subspace, FSC (Gan et al., 2006; Gan and Wu, 2008), FCS (Wu et al., 2005), and ESSC (Deng et al., 2010) are proposed. Whereas, the above algorithms fail to consider the number of iteration steps in the iteration process so that when minimizing the objective function, there are more iteration steps. We recently proposed a new FCM clustering algorithm based on local information and membership linking (FCM_SICM) to overcome the above problem (Wang et al., 2020). In this approach, all membership values before this iteration are summed (called membership linking) and integrated into the FCM as the denominator of the objective function, thus reducing the value of the objective function to reduce the number of iterations. However, when the image is heavily contaminated with noise, the algorithm shows outliers in the membership degrees, which in turn makes the values of the membership linking appear abnormal, thus causing the algorithm to converge prematurely before reaching the optimal clustering effect and affecting the segmentation accuracy (as discussed in Section 3.2).

Although the above algorithms are robust to noise, the following issues have existed. (1) The local or non-local information has poor suppression ability to noise, and the algorithm appears under-segmentation as the image is seriously contaminated by noise. (2) Although the FCM_SICM algorithm based on membership linking can effectively reduce the number of iterations, the algorithm prematurely converges with abnormal membership values, reducing the algorithm's segmentation accuracy. (3) The above algorithms assign the same weights to each dimension of the image when performing clustering, while for color images, the contribution of different channels to the clustering results may not be the same, so the average idea is not conducive to the segmentation of color images. To solve these problems, a robust fuzzy subspace clustering algorithm with adaptive local variance & non-local spatial information and mean membership linking (FSC_LNML) is proposed for noisy image segmentation. The motives and methods are as follows. Considering the under-segmentation of non-local spatial information while the noise density is too high, we introduce the local variance template and apply it to the image with non-local spatial information to eliminate the under-segmentation. The number of iteration steps in the clustering process is also essential in evaluating efficiency. We introduce the mean membership linking into the objective function to reduce the number of iteration steps and avoid premature convergence. Simultaneously, the original image and the local variance & non-local spatial information intensity difference and its reciprocal are utilized to adaptively constrain the original image and the local variance & non-local spatial information. Consider that in clustering, the influence of pixels between different dimensions may not be equal. Assigning appropriate weights to each dimension can improve the performance of color image segmentation. Therefore, this paper introduces subspace clustering into the objective function, assigns appropriate weights to the data of each dimension, and improves the segmentation performance of color images.

In summary, our proposed algorithm has three advantages over general clustering approaches. (1) Introducing a local variance template in the non-local spatial information to eliminate the under-segmentation of the non-local spatial information. (2) Using the mean membership linking as the denominator of the objective function to reduce the iteration steps and solve the convergence problem of the objective function before the algorithm reaches the optimal solution. (3) Assigning appropriate weights to each image dimension to improve the segmentation performance of color images.

The rest of this paper is organized as follows. Section 2 reviews the traditional FCM clustering algorithm, fuzzy subspace clustering algorithm, and non-local spatial information. The proposed method and its implementation are described in detail in Section 3. The experimental results for grayscale images and authentic color images and the parameter choice are discussed in Section 4. In Section 5, a comparison of the proposed method, FSC_LNML, with other similar studies is presented. Finally, conclusions are given in Section 6.

2. Related algorithms

2.1. Standard FCM clustering algorithm

The FCM clustering algorithm converges the objective function through multiple iterations and assigns the data to the appropriate clustering cluster. The objective function is

$$J_{FCM} = \sum_{i=1}^k \sum_{j=1}^N u_{ij}^m \|y_j - c_i\|^2, \sum_{i=1}^k u_{ij} = 1 \quad (1)$$

where k is the number of clusters, N is the total number of data, u_{ij} is the membership of the j th pixel to the i th cluster, m is the weighted index of u_{ij} , c_i is the group of the i th cluster.

Using Lagrangian multiplier method J_{FCM} is minimized by u_{ij} and c_i

$$u_{ij} = \sum_{r=1}^k \left(\frac{\|y_j - c_r\|}{\|y_j - c_r\|} \right)^{\frac{-2}{(m-1)}} \quad (2)$$

$$c_i = \frac{\sum_{j=1}^N u_{ij}^m y_j}{\sum_{j=1}^N u_{ij}} \quad (3)$$

2.2. The fuzzy subspace clustering algorithm

The standard FCM algorithm processes the data of all dimensions equally, but in clustering, the influence of pixels between different dimensions may not be equal. By assigning appropriate weights to each dimension, color image segmentation can be improved (Gan et al., 2006; Wang et al., 2013; Gan and Wu, 2008). Thus the fuzzy subspace clustering (FSC) algorithm was proposed by Gan et al. (2006), which clusters high-dimensional datasets by assigning appropriate weights to data of different dimensions. The objective function is

$$J_{FSC} = \sum_{i=1}^k \sum_{j=1}^N u_{ij} \sum_{z=1}^D w_{iz}^\tau (y_{jz} - c_{iz})^2 + \gamma \sum_{i=1}^k \sum_{z=1}^D w_{iz}^\tau, \sum_{i=1}^k u_{ij} = 1, \sum_{z=1}^D w_{iz} = 1 \quad (4)$$

where D is the data dimension, w_{iz}^τ is the fuzzy weighting factor, τ is the fuzzy index, and is always set $\tau > 1$.

Using Lagrangian multiplier method, u_{ij} , w_{iz} and c_{iz} are updated by

$$c_{iz} = \frac{\sum_{j=1}^N u_{ij} y_j}{\sum_{j=1}^N u_{ij}} \quad (5)$$

$$w_{iz} = \frac{\left(\sum_{j=1}^N u_{ij} (y_{jz} - c_{iz})^2 + \gamma \right)^{\frac{1}{\tau-1}}}{\sum_{z=1}^D \left(\sum_{j=1}^N u_{ij} (y_{jz} - c_{iz})^2 + \gamma \right)^{\frac{1}{\tau-1}}} \quad (6)$$

$$u_{ij} = \begin{cases} 1, \sum_{z=1}^D w_{iz}^\tau (y_{jz} - c_{iz})^2 \leq \sum_{z=1}^D w_{iz}^\tau (y_{jz} - c_{pz})^2, p = 1, 2, \dots, k \\ 0, \text{otherwise} \end{cases} \quad (7)$$

It is known from Eq. (4) that although FSC assigns different weights to each dimension, it only considers intra-class information but ignores inter-class information. Therefore, the objective function needs to be improved. The enhanced soft subspace clustering (ESSC) was proposed by Deng et al. (2010), which integrates intra-cluster and inter-cluster information. The objective function of ESSC can be formulated as

$$J_{ESSC} = \sum_{i=1}^k \sum_{j=1}^N u_{ij}^m \sum_{z=1}^D w_{iz} (y_{jz} - c_{iz})^2 + \gamma \sum_{i=1}^k \sum_{z=1}^D w_{iz} \ln w_{iz} - \eta \sum_{i=1}^k \left(\sum_{j=1}^N u_{ij}^m \right) \sum_{z=1}^D w_{iz} (c_{iz} - c_{lz})^2 \quad (8)$$

where c_{lz} is the global center of the sample, γ and η are used to control the influence of entropy and weight on cluster separation, respectively.

2.3. Non-local spatial information

Although FSC and ESSC assign different weight values to data of different dimensions, they are less robust to noise since the spatial information of the data is not considered in the clustering process. Inspired by non-local filtering (Buades et al., 2008), a fuzzy c-means clustering algorithm (FCM_NLS) based on non-local spatial information was proposed by Zhao et al. (2011). This algorithm introduces non-local information into the objective function of FCM to enhance the robustness to noise. The objective function of FCM_NLS is expressed as follows

$$J_{FCM_NLS} = \sum_{i=1}^k \sum_{j=1}^N u_{ij}^m \|y_j - c_i\|^2 + \beta \sum_{i=1}^k \sum_{j=1}^N u_{ij}^m \|\bar{y}_j - c_i\|^2, \sum_{i=1}^k u_{ij} = 1 \quad (9)$$

For the j th pixel, its non-local spatial information \bar{y}_j is computed by the following formula

$$\bar{y}_j = \frac{1}{Z_j} \sum_{y_q \in R_j} y_q \exp \left(\frac{-\|y(N_j) - y(N_q)\|_{2,\nu}^2}{h^2} \right) \quad (10)$$

$$Z_j = \sum_{y_q \in R_j} \exp \left(\frac{-\|y(N_j) - y(N_q)\|_{2,\nu}^2}{h^2} \right) \quad (11)$$

where R_j denotes a $S \times S$ search window centered at the j th pixel, y_q is the q th pixel in R_j of $S \times S$ region centered on a pixel y_j , $y(N_j)$ and $y(N_q)$ are the $l \times l$ local pixel blocks whose center pixels are y_j and y_q respectively, ν is the standard deviation of the Gaussian kernel (Buades et al., 2008), h is the filtering degree parameter which controls the decay of the exponential function. The disadvantage of FCM_NLS is that it cannot perform the adaptive calculation h . Therefore, Zhao (2013) successively proposed an adaptive non-local spatial information algorithm (FCM_SNLS) to calculate non-local details of the data adaptively. The calculation formula is

$$h_i = \|y(N_j) - y(N_{j_l})\|_{2,\nu} \quad (12)$$

where the j_l th pixel is located in the search window R_j and denotes the l th nearest neighbor pixel of the j th pixel.

3. Proposed method

The summary of the above analysis is as follows. (1) Although FCM, FSC and ESSC are simple, they fail to consider the spatial information of the image and thus have poor robustness to noise. (2) FCM_NLS and FCM_SNLS incorporate the non-local spatial information into the objective function to enhance robustness. However, as the noise density increases, the algorithm exists under-segmentation, and the details of the original image are lost and the edges are blurred in obtaining the non-local spatial information. (3) Since the objective function has a significant value in the clustering process, it leads to many iteration steps. This paper proposes a new local variance template to overcome the under-segmentation of non-local spatial information and preserve the image's detail information and edge features to some extent. Then local variance & non-local spatial information is integrated into fuzzy subspace clustering, and an appropriate weight is assigned to each dimension to improve image segmentation performance. Finally, the mean membership linking is utilized as the denominator of the objective function to reduce iteration steps.

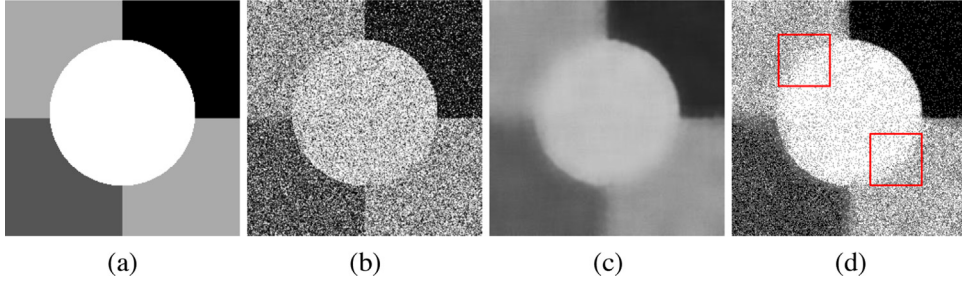


Fig. 1. Segmentation results of FCM_NLS. (a) Original image; (b) Noise image; (c) Corresponding non-local information ($l = 7$, $s = 15$, $v = 4$, $g = 15$); (d) Segmentation result of FCM_NLS.

3.1. The local variance & non-local spatial information

For images seriously damaged by noise, the pixel values are randomly distributed due to the uncertainty of noise, and it is challenging to segment them thoroughly by using the general clustering method. Although the non-local spatial information eliminates the noise interference in some extent, the under-segmentation phenomenon also exists when the noise density is higher. Fig. 1 shows the segmentation results of the FCM_NLS (Zhao et al., 2011) in a high-density noise environment, where FCM_NLS incorporates only the non-local spatial information into the FCM.

In Fig. 1, we can see that primarily noisy pixels are processed by non-local information. However, a few noisy pixels in (b) are over-preserved, resulting in under-segmentation in (d). Moreover, the high-density noise environment makes FCM_NLS lose detailed information and edge blurring during segmentation, as shown in the red rectangular box in (d). It is due to the uncertainty of the noise leading to a random distribution of pixels, which are considered valuable information and are retained in the clustering process. During the smoothing process, the non-local spatial information makes the image detail information lost and poorly maintained at the edges, resulting in blurred boundaries. Therefore, it is necessary to find a method that can solve the under-segmentation phenomenon of non-local spatial information and retain the details and edge information of the image in some extent. This paper proposes a local variance template to address the issues mentioned above. The new local variance information and non-local spatial information are expressed as

$$\xi_{jz} = (1 - p_{jz}) \bar{M}_{jz} + p_{jz} \bar{y}_{jz} \quad (13)$$

where p_{jz} is the weight coefficient that controls the non-local spatial information and its local mean value, \bar{M}_{jz} is the local mean of \bar{y}_{jz} , calculated by the following formula

$$\bar{M}_{jz} = \frac{1}{(2n+1)(2l+1)} \sum_{\bar{y}_{qz} \in N_{l \times n}} \bar{y}_{qz} \quad (14)$$

$$q \neq j$$

where \bar{y}_{qz} is the q th pixel of the z th channel in the $l \times n$ local pixel window $N_{l \times n}$ centered on pixel \bar{y}_{jz} . In general, in local information operations, the search window is a rectangle of equal width and height, so set $l = n$ and Eq. (14) can be denoted as

$$\bar{M}_{jz} = \frac{1}{(2n+1)^2} \sum_{\bar{y}_{qz} \in N_{l \times n}} \bar{y}_{qz} \quad (15)$$

$$q \neq j$$

Many experiments have shown that settings $n = 5$ can suppress isolated noise pixels and maintain image details and edge information. Next, calculate the weight coefficient p_{jz} . In mathematics, the variance is the degree of deviation from the center in statistics, which is utilized to measure the volatility of the data. For a noisy image, when the local variance is relatively small, it means that the local area in the image

belongs to the grayscale flat area, and the gray value of each pixel is not much different. That is, the pixel is less disturbed by noise. Conversely, when the local variance is relatively large, it means that the local area in the image belongs to the high-frequency area, and the gray value of each pixel is somewhat different. That is, the pixel is seriously damaged by noise. Therefore, this paper employs the local variance as the weight parameter to constrain the non-local spatial information and its local mean information, then p_{jz} is shown as

$$p_{jz} = \frac{Q_{jz}}{V_{jz} + \sigma} \quad (16)$$

where Q_{jz} and V_{jz} are the global mean and local variance of the non-local spatial information, respectively, σ is the control parameter. The local variance V_{jz} can be indicated as:

$$V_{jz} = \frac{1}{(2n+1)^2} \sum_{\bar{y}_{qz} \in N_{l \times n}} (\bar{y}_{qz} - \bar{M}_{jz})^2 \quad (17)$$

$$q \neq j$$

where \bar{M}_{jz} is the local mean calculated by Eq. (15). Note that the p_{jz} needs to be normalized to the interval $[0, 1]$, then:

$$\vartheta_{jz} = \frac{p_{jz} - p_{\min}}{p_{\max} - p_{\min}} \quad (18)$$

where p_{\min} and p_{\max} are the minimum and maximum values of all p_{jz} , respectively. Finally, the local variance template and non-local spatial information are equaled as

$$\xi_{jz} = (1 - \vartheta_{jz}) \bar{M}_{jz} + \vartheta_{jz} \bar{y}_{jz} \quad (19)$$

For showing that the noise suppression ability of the proposed local variance template & non-local spatial information is better than that of a single non-local spatial information (FCM_NLS), three different synthetic images are generated using the Gibbs sampler, and the images are contaminated with 5% mixture of noise. Then the performance of the two algorithms is discussed in three cases. In Figs. 2, 3, and 4: (a) is the noise image; (b) is the pixel value of the region marked with a red rectangular box, where the gray background is the noise pixel; (c)–(e) are the membership values of the three clusters after segmentation with FCM_NLS; (f)–(h) are the membership values of the three clusters after segmentation with the proposed algorithm. The final segmentation results of the three synthetic images by the FCM_NLS algorithm and the proposed algorithm are shown in Fig. 5.

Case 1: The central pixel of the region has no noise, and its neighboring pixels are corrupted by noise. The pixel values of the 5×5 area marked in Fig. 2(a) are shown in Fig. 2(b), and the noise pixel values in the region are 112, 0, 5, 1, and 134, which are different from the central pixel value (pixel value is 38). The FCM_NLS and the proposed algorithm converge after the 39th and 12th iterations. Theoretically, the membership values belonging to a particular class after iteration should be greater than 0.5. However, the FCM_NLS algorithm has one noisy pixel and three non-noisy pixels with membership values less than 0.5 after iteration (as shown in the red rectangular box marked in

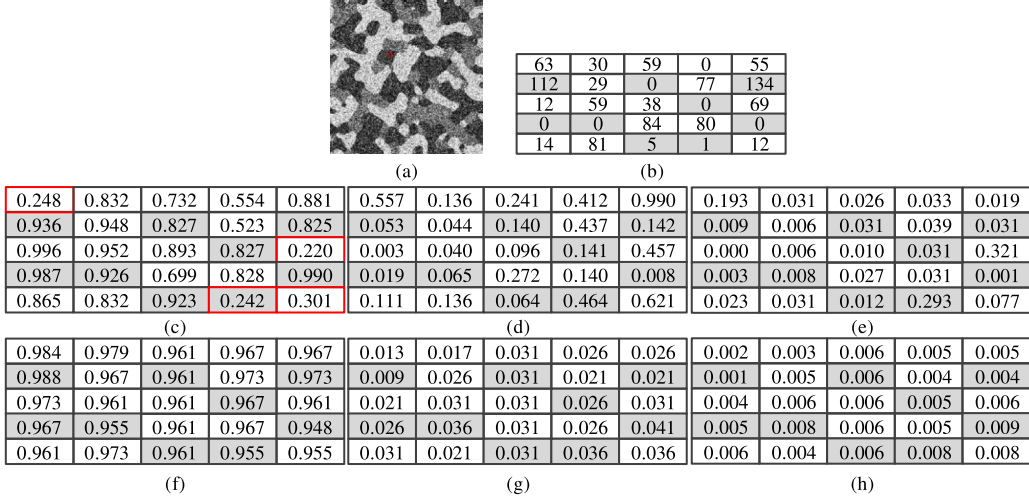


Fig. 2. Membership values of FCM_NLS and the proposed algorithm: (a) the noise image; (b) the pixel value of the region marked with a red rectangular box; (c)–(e) the membership values of the three clusters after segmentation with FCM_NLS; (f)–(h) the membership values of the three clusters after segmentation with the proposed algorithm.

Fig. 2(c)), indicating that the non-local spatial information is less robust to noise and fails to suppress noise better. After the proposed method is iterated, the membership values of all pixels are more significant than 0.9, which indicates that the algorithm can effectively suppress the noise and achieve better pixel clustering.

Case 2: The central pixel of the region is corrupted by noise, and its neighboring pixels are free from noise. In this case, the gray value of the center pixel is 27, which is different from its adjacent pixels. The FCM_NLS and the proposed algorithm converge after the 43rd and 11th iterations. As shown in **Fig. 3(c)**, the FCM_NLS has 9 pixels misclassified after the iterations, among which the central pixel is also not correctly classified, while the final membership values of the proposed algorithms are both greater than 0.5. This indicates that the proposed algorithm has the same noise suppression capability in this case.

Case 3: In cases 1 and 2, the pixels of the given local window are homogeneous, i.e., the pixels belong to the same region, and in fact, there are also some pixels located at the boundaries of the object. As shown in case 3, **Fig. 4(b)** shows the pixels in two regions (black background region for the first class of pixels; white background region for the second class of pixels; noisy pixel background is gray). The FCM_NLS and the proposed algorithm converge after the 52nd and 15th iterations. As shown in **Fig. 4(c)** and (d), the FCM_NLS algorithm fails to classify 9 pixels correctly after iteration, while the final membership values of the proposed algorithm are both greater than 0.5, indicating that the proposed algorithm can segment the noisy image better while maintaining the edge information of the image.

In this paper, the local variance template and non-local spatial information is incorporated as follows

$$\begin{aligned} J_{FSC_LNML}^{(a)} = & \sum_{i=1}^k \sum_{j=1}^N \left(u_{ij}^{(a)} \right)^m \left[\sum_{z=1}^D \left(w_{iz}^{(a)} \right)^\tau \left(\alpha_{jz} \|y_{jz} - c_{iz}^{(a)}\|^2 \right. \right. \\ & \left. \left. + \beta_{jz} \|\xi_{jz} - c_{iz}^{(a)}\|^2 \right) \right] + \gamma \sum_{i=1}^k \sum_{z=1}^D \left(w_{iz}^{(a)} \right)^\tau, \sum_{i=1}^k u_{ij} = 1, \sum_{z=1}^D w_{iz}^\tau = 1 \end{aligned} \quad (20)$$

where D is the data dimension, $\left(w_{iz}^{(a)} \right)^\tau$ is the fuzzy weighting factor, τ is the fuzzy index, and is always set $\tau > 1$, ξ_{jz} is local variance and non-local spatial information, γ is weight regularization parameter, α_{jz} and β_{jz} are the constraints of the original image and local variance and non-local spatial information, respectively.

3.2. The way to reduce the number of iteration steps

Many clustering algorithms solve for optimality by iteratively minimizing the objective function. However, the number of iterative steps

is not considered in many cases. It was found in Wang et al. (2020) that for the i th cluster, one can apply the summary of membership computed in the previous iterations to reduce the iteration steps, which is called membership linking M

$$M = \sum_{e=1}^N u_{ie}^{(a-1)} \quad (21)$$

where a is the number of iterations steps. For avoiding the convergence of the algorithm before the clustering result reaches the optimum, modify M to logarithmic form

$$M = \ln^2 \left(\sum_{e=1}^N u_{ie}^{(a-1)} + 1 \right) \quad (22)$$

Nevertheless, when the image pixel is seriously corrupted by noise, there are too many outliers of membership degree in the iteration process. Thus the value of the membership linking also appears abnormal, leading to premature convergence of the objective function. **Fig. 6** shows the distribution of the membership values after convergence of the algorithm when there are outliers in the membership linking. Since the FCM_NLS algorithm has under-segmentation in the mixed noise environment, which makes the membership value abnormal in the clustering process (as shown in Section 3.1), introducing the membership linking into the FCM_NLS objective function (denoted as FCM_NLSM) can objectively illustrate the impact on the convergence of the algorithm when the membership linking has outliers. **Fig. 6** (a) and (b) show the original and noisy images; (c) and (d) show the pixel values of the 5×5 regions marked by the red rectangular boxes in (a) and (b), where the gray background is the noisy pixels; (e)–(g) show the membership values of the FCM_NLSM algorithm after the 1st, 2nd, and 12th iterations.

All pixels in **Fig. 6(d)** should be clustered as white, and the corresponding membership value should be greater than 0.5. The algorithm converges after the 12th iteration. It is noteworthy that outliers less than 0.5 appear at noisy and non-noisy points after convergence, which indicates that outliers in the membership linking affect the algorithm's convergence and make the algorithm converge prematurely before reaching the optimum, affecting the clustering effect. Therefore, it is essential to find an effective method to reduce the adverse impact of outliers. In this paper, the mean value of each member before this iteration is calculated and then summed to minimize the effect of outliers, called the mean membership linking. It expressed as

$$M = \ln^2 \left(\sum_{e=1}^N \text{mean}(u_{ie}^{(a-1)}) + 1 \right) \quad (23)$$

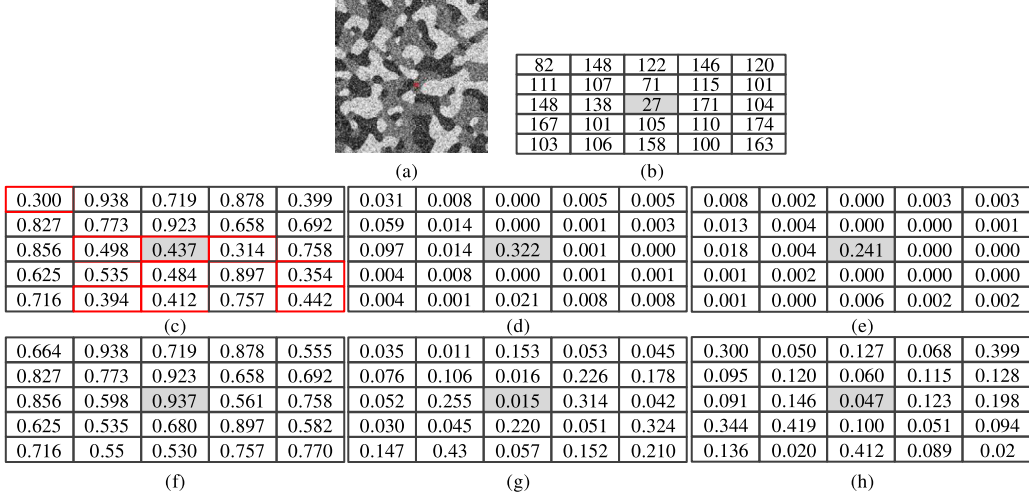


Fig. 3. Membership values of FCM_NLS and the proposed algorithm: (a) the noise image; (b) the pixel value of the region marked with a red rectangular box; (c)–(e) the membership values of the three clusters after segmentation with FCM_NLS; (f)–(h) the membership values of the three clusters after segmentation with the proposed algorithm.

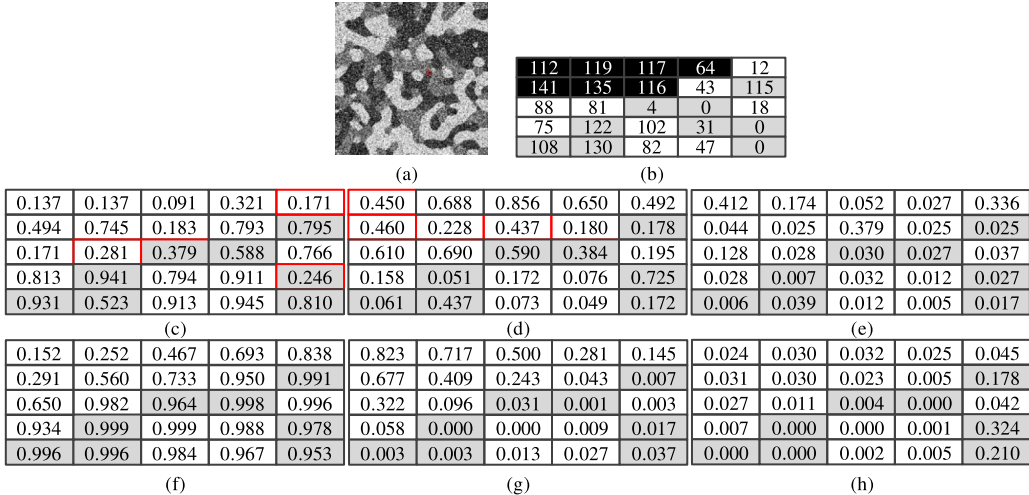


Fig. 4. Membership values of FCM_NLS and the proposed algorithm: (a) the noise image; (b) the pixel value of the region marked with a red rectangular box; (c)–(e) the membership values of the three clusters after segmentation with FCM_NLS; (f)–(h) the membership values of the three clusters after segmentation with the proposed algorithm.

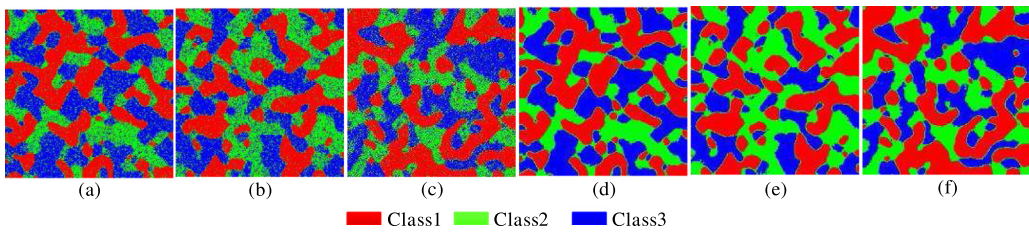


Fig. 5. The final segmentation results of the FCM_NLS algorithm and the proposed algorithm for the three synthetic images: (a)–(c) FCM_NLS segmentation results; (d)–(f) Segmentation results of the proposed algorithm.

Fig. 6(h)–(j) show the distribution of the membership values after the convergence of the proposed algorithm. The algorithm converges after the 9th iteration. It can be seen that the noisy pixels in **Fig. 6(b)** are clustered as white, and the corresponding membership values are all greater than 0.9, indicating that the mean membership linking can effectively eliminate the outlier interference.

Now, the objective function $J_{FSC_LNML}^{(a)}$ is given as in **Box I**

3.3. Adaptive constraint weight α_{jz} and β_{jz}

In Eq. (24), α_{jz} and β_{jz} are the constraints of the original image and local variance & non-local spatial information, respectively. Suppose the original image is heavily contaminated with noise. In that case, a more significant value β_{jz} and a smaller value α_{jz} are set, which allows the local variance & non-local spatial information to influence

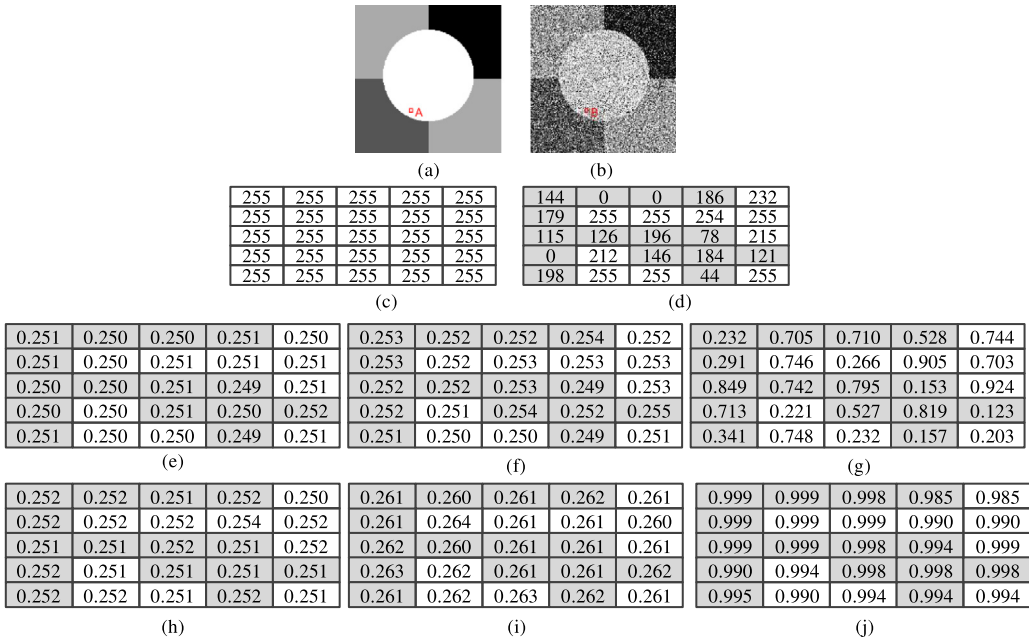


Fig. 6. Membership degrees of FCM_NLSM variant and proposed method. (a) Original image; (b) Noise image; (c) Grayscale values of red marked area in (a); (d) Grayscale values of red marked area in (b); (e)–(g) Variants of FCM_NLS; (h)–(j) Proposed method.

$$J_{FSC_LNML}^{(a)} = \frac{\sum_{i=1}^k \sum_{j=1}^N \left(u_{ij}^{(a)}\right)^m \left[\sum_{z=1}^D \left(w_{iz}^{(a)}\right)^T \left(\alpha_{jz} \left\|y_{jz} - c_{iz}^{(a)}\right\|^2 + \beta_{jz} \left\|\xi_{jz} - c_{iz}^{(a)}\right\|^2 \right) \right] + \gamma \sum_{i=1}^k \sum_{z=1}^D \left(w_{iz}^{(a)}\right)^T}{\ln^2 \left(\sum_{e=1}^N \text{mean}(u_{ie}^{(a-1)}) + 1\right)}, \sum_{i=1}^k u_{ij} = 1, \sum_{z=1}^D w_{iz}^{(a)} = 1 \quad (24)$$

Box I.

the segmentation results better while preserving the original image in some extent. On the contrary, as noise density decreases, a significant α_{jz} and small β_{jz} must ensure that the original image information is fully utilized. Therefore, if fixed α_{jz} and β_{jz} are set in all images, the flexibility of the algorithm is low. The better approach is to adaptively apply different constraints between pixels, depending on the image itself.

Following Wang et al. (2020), this paper utilizes the intensity difference between y_{jz} and ξ_{jz} constrains the original image and local variance & non-local spatial information. For a noisy image, the more severe the pixel y_{jz} is interfered with by noise, the larger $|y_{jz} - \xi_{jz}|$, the more significant the intensity difference between the original image and local variance & non-local spatial information, and vice versa, the smaller $|y_{jz} - \xi_{jz}|$. When the value $|y_{jz} - \xi_{jz}|$ is more considerable, its reciprocal is smaller, so it is appropriate to use $|y_{jz} - \xi_{jz}|$ and $1/|y_{jz} - \xi_{jz}|$ to constrain the original image and local variance & non-local spatial information, respectively. Then, there is

$$\beta_{jz} = |y_{jz} - \xi_{jz}| \quad (25)$$

$$\alpha_{jz} = \frac{1}{|y_{jz} - \xi_{jz}|} \quad (26)$$

To prevent α_{jz} and β_{jz} from approaching 0 and infinity, express α_{jz} and β_{jz} as

$$\beta_{jz} = k |y_{jz} - \xi_{jz}| + eps \quad (27)$$

$$\alpha_{jz} = \frac{1}{k |y_{jz} - \xi_{jz}| + eps} \quad (28)$$

Considering that $|y_{jz} - \xi_{jz}|$ is only related to the pixels in the original image and the local variance & non-local spatial information, and does not change during the iteration process, to reduce the computational complexity of the algorithm, it can be calculated in advance, expressed as

$$\Delta y_{jz} = k |y_{jz} - \xi_{jz}| + eps \quad (29)$$

where k and eps are to prevent the value Δy from becoming too large or zero. Many experiments have proved that $k = 20$ can get better segmentation results.

Finally, the objective function $J_{FSC_LNML}^{(a)}$ of the proposed method FSC_LNML is assumed as given in Box II.

3.4. Iterative formula calculation

The Lagrange multiplier method is employed to solve the iterative formula. Lagrange function F is as given in Box III where λ_{j1} and λ_{j2} are Lagrange multiplier. Firstly, derive the equation of $u_{ij}^{(a)}$. Take the partial derivative of Eq. (31) over $u_{ij}^{(a)}$

$$\begin{aligned} \frac{\partial F}{\partial u_{ij}^{(a)}} &= \frac{m \left(u_{ij}^{(a)}\right)^{m-1} \left[\sum_{z=1}^D \left(w_{iz}^{(a)}\right)^T \left(\frac{1}{\Delta y_{jz}} \left\|y_{jz} - c_{iz}^{(a)}\right\|^2 + \Delta y_{jz} \left\|\xi_{jz} - c_{iz}^{(a)}\right\|^2 \right) \right]}{\ln^2 \left(\sum_{e=1}^N \text{mean}(u_{ie}^{(a-1)}) + 1\right)} - \lambda_{j1} = 0 \\ &\Rightarrow \frac{m \left(u_{ij}^{(a)}\right)^{m-1} \left[\sum_{z=1}^D \left(w_{iz}^{(a)}\right)^T \left(\frac{1}{\Delta y_{jz}} \left\|y_{jz} - c_{iz}^{(a)}\right\|^2 + \Delta y_{jz} \left\|\xi_{jz} - c_{iz}^{(a)}\right\|^2 \right) \right]}{\ln^2 \left(\sum_{e=1}^N \text{mean}(u_{ie}^{(a-1)}) + 1\right)} = \lambda_{j1} \\ &\Rightarrow u_{ij}^{(a)} = \left\{ \frac{\lambda_{j1} \ln^2 \left(\sum_{e=1}^N \text{mean}(u_{ie}^{(a-1)}) + 1\right)}{m \left[\sum_{z=1}^D \left(w_{iz}^{(a)}\right)^T \left(\frac{1}{\Delta y_{jz}} \left\|y_{jz} - c_{iz}^{(a)}\right\|^2 + \Delta y_{jz} \left\|\xi_{jz} - c_{iz}^{(a)}\right\|^2 \right) \right]} \right\}^{\frac{1}{m-1}} \end{aligned}$$

$$J_{FSC_LNML}^{(a)} = \frac{\sum_{i=1}^k \sum_{j=1}^N \left(u_{ij}^{(a)}\right)^m \left[\sum_{z=1}^D \left(w_{iz}^{(a)}\right)^\tau \left(\frac{1}{\Delta y_{jz}} \|y_{jz} - c_{iz}^{(a)}\|^2 + \Delta y_{jz} \|\xi_{jz} - c_{iz}^{(a)}\|^2 \right) \right] + \gamma \sum_{i=1}^k \sum_{z=1}^D \left(w_{iz}^{(a)}\right)^\tau}{\ln^2 \left(\sum_{e=1}^N \text{mean}(u_{ie}^{(a-1)}) + 1\right)}, \sum_{i=1}^k u_{ij} = 1, \sum_{z=1}^D w_{iz} = 1 \quad (30)$$

Box II.

$$F = \frac{\sum_{i=1}^k \sum_{j=1}^N \left(u_{ij}^{(a)}\right)^m \left[\sum_{z=1}^D \left(w_{iz}^{(a)}\right)^\tau \left(\frac{1}{\Delta y_{jz}} \|y_{jz} - c_{iz}^{(a)}\|^2 + \Delta y_{jz} \|\xi_{jz} - c_{iz}^{(a)}\|^2 \right) \right] + \gamma \sum_{i=1}^k \sum_{z=1}^D \left(w_{iz}^{(a)}\right)^\tau}{\ln^2 \left(\sum_{e=1}^N \text{mean}(u_{ie}^{(a-1)}) + 1\right)} + \sum_{j=1}^N \lambda_{j1} \left(1 - \sum_{i=1}^k u_{ij}^{(a)}\right) + \sum_{j=1}^N \lambda_{j2} \left(1 - \sum_{z=1}^D w_{iz}^{(a)}\right) \quad (31)$$

Box III.

$$\Rightarrow u_{ij}^{(a)} = \left(\frac{\lambda_{j1}}{m}\right)^{\frac{1}{m-1}} \frac{1}{\left[\frac{\sum_{z=1}^D \left(w_{iz}^{(a)}\right)^\tau \left(\frac{1}{\Delta y_{jz}} \|y_{jz} - c_{iz}^{(a)}\|^2 + \Delta y_{jz} \|\xi_{jz} - c_{iz}^{(a)}\|^2\right)}{\ln^2 \left(\sum_{e=1}^N \text{mean}(u_{ie}^{(a-1)}) + 1\right)}\right]^{\frac{1}{m-1}}} \quad (32)$$

Take the partial derivative of Eq. (31) over λ_{j1}

$$\frac{\partial F}{\partial \lambda_{j1}} = 0 \Rightarrow \sum_{i=1}^k u_{ij}^{(a)} = 1 \quad (33)$$

Substitute Eq. (33) into Eq. (32)

$$\sum_{i=1}^k u_{ij}^{(a)} = \left(\frac{\lambda_{j1}}{m}\right)^{\frac{1}{m-1}} \sum_{i=1}^k \frac{1}{\left[\frac{\sum_{z=1}^D \left(w_{iz}^{(a)}\right)^\tau \left(\frac{1}{\Delta y_{jz}} \|y_{jz} - c_{iz}^{(a)}\|^2 + \Delta y_{jz} \|\xi_{jz} - c_{iz}^{(a)}\|^2\right)}{\ln^2 \left(\sum_{e=1}^N \text{mean}(u_{ie}^{(a-1)}) + 1\right)}\right]^{\frac{1}{m-1}}} = 1 \quad (34)$$

$$\Rightarrow \left(\frac{\lambda_{j1}}{m}\right)^{\frac{1}{m-1}} = \frac{1}{\sum_{i=1}^k \left[\frac{1}{\left[\frac{\sum_{z=1}^D \left(w_{iz}^{(a)}\right)^\tau \left(\frac{1}{\Delta y_{jz}} \|y_{jz} - c_{iz}^{(a)}\|^2 + \Delta y_{jz} \|\xi_{jz} - c_{iz}^{(a)}\|^2\right)}{\ln^2 \left(\sum_{e=1}^N \text{mean}(u_{ie}^{(a-1)}) + 1\right)}\right]^{\frac{1}{m-1}}}\right]} \quad (35)$$

Substitute Eq. (35) into Eq. (32)

$$u_{ij}^{(a)} = \frac{1}{\sum_{i=1}^k \left[\frac{1}{\left[\frac{\sum_{z=1}^D \left(w_{iz}^{(a)}\right)^\tau \left(\frac{1}{\Delta y_{jz}} \|y_{jz} - c_{iz}^{(a)}\|^2 + \Delta y_{jz} \|\xi_{jz} - c_{iz}^{(a)}\|^2\right)}{\ln^2 \left(\sum_{e=1}^N \text{mean}(u_{ie}^{(a-1)}) + 1\right)}\right]^{\frac{1}{m-1}}}\right]} \times \frac{1}{\left[\frac{\sum_{z=1}^D \left(w_{iz}^{(a)}\right)^\tau \left(\frac{1}{\Delta y_{jz}} \|y_{jz} - c_{iz}^{(a)}\|^2 + \Delta y_{jz} \|\xi_{jz} - c_{iz}^{(a)}\|^2\right)}{\ln^2 \left(\sum_{e=1}^N \text{mean}(u_{ie}^{(a-1)}) + 1\right)}\right]^{\frac{1}{m-1}}} \quad (36)$$

$$\Rightarrow u_{ij}^{(a)} = \frac{1}{\sum_{r=1}^k \left[\frac{1}{\left[\frac{\sum_{z=1}^D \left(w_{iz}^{(a)}\right)^\tau \left(\frac{1}{\Delta y_{jz}} \|y_{jz} - c_{iz}^{(a)}\|^2 + \Delta y_{jz} \|\xi_{jz} - c_{iz}^{(a)}\|^2\right)}{\ln^2 \left(\sum_{e=1}^N \text{mean}(u_{ie}^{(a-1)}) + 1\right)}\right]^{\frac{1}{m-1}}}\right]} \quad (37)$$

Next, derive the equation of $c_{iz}^{(a)}$. Take the partial derivative of Eq. (31) over $c_{iz}^{(a)}$

$$\begin{aligned} \frac{\partial F}{\partial c_{iz}^{(a)}} &= -2 \sum_{j=1}^N \left(u_{ij}^{(a)}\right)^m \left(w_{iz}^{(a)}\right)^\tau \left(\frac{1}{\Delta y_{jz}} \|y_{jz} - c_{iz}^{(a)}\| + \Delta y_{jz} \|\xi_{jz} - c_{iz}^{(a)}\| \right) = 0 \\ &\Rightarrow \sum_{j=1}^N \left(u_{ij}^{(a)}\right)^m \frac{1}{\Delta y_{jz}} y_{jz} - \sum_{j=1}^N \left(u_{ij}^{(a)}\right)^m \frac{1}{\Delta y_{jz}} c_{iz}^{(a)} + \sum_{j=1}^N \left(u_{ij}^{(a)}\right)^m \Delta y_{jz} \xi_{jz} \\ &\quad - \sum_{j=1}^N \left(u_{ij}^{(a)}\right)^m \Delta y_{jz} c_{iz}^{(a)} = 0 \\ &\Rightarrow \sum_{j=1}^N \left(u_{ij}^{(a)}\right)^m \left(\frac{y_{jz}}{\Delta y_{jz}} + \Delta y_{jz} \xi_{jz} \right) = c_{iz}^{(a)} \sum_{j=1}^N \left(u_{ij}^{(a)}\right)^m \left(\frac{1}{\Delta y_{jz}} + \Delta y_{jz} \right) \end{aligned} \quad (38)$$

$$\Rightarrow c_{iz}^{(a)} = \frac{\sum_{j=1}^N \left(u_{ij}^{(a)}\right)^m \left(\frac{y_{jz}}{\Delta y_{jz}} + \Delta y_{jz} \xi_{jz} \right)}{\sum_{j=1}^N \left(u_{ij}^{(a)}\right)^m \left(\frac{1}{\Delta y_{jz}} + \Delta y_{jz} \right)} \quad (39)$$

Finally, derive the equation of $w_{iz}^{(a)}$. Take the partial derivative of Eq. (31) over $w_{iz}^{(a)}$

$$\begin{aligned} \frac{\partial F}{\partial w_{iz}^{(a)}} &= \tau \left(w_{iz}^{(a)}\right)^{\tau-1} \sum_{j=1}^N \left(u_{ij}^{(a)}\right)^m \left[\left(\frac{1}{\Delta y_{jz}} \|y_{jz} - c_{iz}^{(a)}\|^2 + \Delta y_{jz} \|\xi_{jz} - c_{iz}^{(a)}\|^2 \right) \right] + \gamma \tau \left(w_{iz}^{(a)}\right)^{\tau-1} - \lambda_{j2} = 0 \\ &\Rightarrow \tau \left(w_{iz}^{(a)}\right)^{\tau-1} \sum_{j=1}^N \left(u_{ij}^{(a)}\right)^m \left[\left(\frac{1}{\Delta y_{jz}} \|y_{jz} - c_{iz}^{(a)}\|^2 + \Delta y_{jz} \|\xi_{jz} - c_{iz}^{(a)}\|^2 \right) \right] \\ &\quad + \gamma \tau \left(w_{iz}^{(a)}\right)^{\tau-1} = \lambda_{j2} \end{aligned}$$

$$\Rightarrow w_{iz}^{(a)} = \left\{ \frac{\lambda_{j2}}{\tau \sum_{j=1}^N \left(u_{ij}^{(a)}\right)^m \left[\left(\frac{1}{\Delta y_{jz}} \|y_{jz} - c_{iz}^{(a)}\|^2 + \Delta y_{jz} \|\xi_{jz} - c_{iz}^{(a)}\|^2 \right) \right] + \tau \gamma} \right\}^{\frac{1}{\tau-1}} \quad (40)$$

$$\Rightarrow w_{iz}^{(a)} = \left(\frac{\lambda_{j2}}{\tau}\right)^{\frac{1}{\tau-1}} \frac{1}{\left\{ \sum_{j=1}^N \left(u_{ij}^{(a)}\right)^m \left[\left(\frac{1}{\Delta y_{jz}} \|y_{jz} - c_{iz}^{(a)}\|^2 + \Delta y_{jz} \|\xi_{jz} - c_{iz}^{(a)}\|^2 \right) \right] + \gamma \right\}^{\frac{1}{\tau-1}}} \quad (41)$$

Take the partial derivative of Eq. (31) over λ_{j2}

$$\frac{\partial F}{\partial \lambda_{j2}} = 0 \Rightarrow \sum_{z=1}^D w_{iz}^{(a)} = 1 \quad (42)$$

Substitute Eq. (42) into Eq. (41)

$$\sum_{z=1}^D w_{iz}^{(a)} = \left(\frac{\lambda_{j2}}{\tau} \right)^{\frac{1}{\tau-1}} \sum_{z=1}^D \frac{1}{\left\{ \sum_{j=1}^N \left(u_{ij}^{(a)} \right)^m \left[\left(\frac{1}{\Delta y_{jz}} \|y_{jz} - c_{iz}^{(a)}\|^2 + \Delta y_{jz} \|\xi_{jz} - c_{iz}^{(a)}\|^2 \right) \right] + \gamma \right\}^{\frac{1}{\tau-1}}} = 1 \quad (43)$$

$$\Rightarrow \left(\frac{\lambda_{j2}}{\tau} \right)^{\frac{1}{\tau-1}} = \frac{1}{\sum_{z=1}^D \frac{1}{\left\{ \sum_{j=1}^N \left(u_{ij}^{(a)} \right)^m \left[\left(\frac{1}{\Delta y_{jz}} \|y_{jz} - c_{iz}^{(a)}\|^2 + \Delta y_{jz} \|\xi_{jz} - c_{iz}^{(a)}\|^2 \right) \right] + \gamma \right\}^{\frac{1}{\tau-1}}}} \quad (44)$$

Substitute Eq. (44) into Eq. (41)

$$w_{iz}^{(a)} = \frac{1}{\sum_{z=1}^D \frac{1}{\left\{ \sum_{j=1}^N \left(u_{ij}^{(a)} \right)^m \left[\left(\frac{1}{\Delta y_{jz}} \|y_{jz} - c_{iz}^{(a)}\|^2 + \Delta y_{jz} \|\xi_{jz} - c_{iz}^{(a)}\|^2 \right) \right] + \gamma \right\}^{\frac{1}{\tau-1}}}} \quad (45)$$

$$w_{iz}^{(a)} = \frac{1}{\sum_{s=1}^D \left\{ \frac{1}{\sum_{j=1}^N \left(u_{ij}^{(a)} \right)^m \left[\left(\frac{1}{\Delta y_{js}} \|y_{js} - c_s^{(a)}\|^2 + \Delta y_{js} \|\xi_{js} - c_s^{(a)}\|^2 \right) \right] + \gamma} \right\}^{\frac{1}{\tau-1}}} \quad (46)$$

Algorithm (Proposed method FSC_LNML).

Input: Original image I ; cluster number k ; minimum error η' ; membership weight index m ; maximum iteration number T ; variance control parameter σ ; fuzzy index τ ; regularization parameter γ ; local window size l ; non-local window size S ; filtering degree parameter h .

1. Normalize the original image $[0, 1]$
2. Compute all non-local information pixels y_{jz} by Eqs. (10)–(11).
3. Compute the local mean of the non-local spatial information \bar{y}_{jz} by Eq. (14).
4. Compute the local variance of the non-local spatial information \bar{y}_{jz} by Eq. (17).
5. Compute the weighting factor p_{jz} by Eq. (16).
6. Compute the normalized parameter ϑ_{jz} by Eq. (18).
7. Compute local variance templates & non-local spatial information ξ_{jz} by Eq. (19).
8. Compute Δy_{jz} by Eq. (29).
9. Initialize the membership matrix $u_{ij}^{(1)}$
10. Repeat
 - a. Update $c_{iz}^{(a)}$ by Eq. (39).
 - b. Update $w_{iz}^{(a)}$ by Eq. (46).
 - c. Update $u_{ij}^{(a)}$ by Eq. (37).
 - d. Update $J_{FSC_LNML}^{(a)}$ by Eq. (30).
 - e. $a = a + 1$.
11. Until $\|J_{FSC_LNML}^{(a)} - J_{FSC_LNML}^{(a-1)}\| \leq \eta', a > 1$.
12. Return Membership degrees $u_{ij}^{(a)}$
13. Assign each pixel to the clustering cluster with the highest membership

3.5. Convergence proof

This section presents the proof of convergence of the proposed algorithm. The goal is to prove that the objective function in Eq. (31) reaches a minimum value. That is, the algorithm converges.

Theorem 1. Let the central matrix $c_{iz}^{(a)}$ and the weight matrix $w_{iz}^{(a)}$ be fixed, and the matrix $u_{ij}^{(a)}$ be a strict local minimum of Eq. (31) if and only if obtained from Eq. (37).

Proof. $u_{ij}^{(a)}$ in Eq. (37) is calculated by taking the derivative of Eq. (31) and setting it zero (see section 3.4 for details). Therefore, $u_{ij}^{(a)}$ is either a minimum or a maximum. Now, if the second partial derivative of Eq. (31) is proved to be positive, it can be shown that $u_{ij}^{(a)}$ obtained from Eq. (37) is a local minimum of Eq. (31). The second derivative of Eq. (31) for $u_{ij}^{(a)}$ is shown below

$$\frac{m(m-1) \left(u_{ij}^{(a)} \right)^{m-2} \left[\sum_{z=1}^D \left(w_{iz}^{(a)} \right)^{\tau} \left(\frac{1}{\Delta y_{jz}} \|y_{jz} - c_{iz}^{(a)}\|^2 + \Delta y_{jz} \|\xi_{jz} - c_{iz}^{(a)}\|^2 \right) \right]}{\ln^2 \left(\sum_{e=1}^N \text{mean}(u_{ie}^{(a-1)}) + 1 \right)} \quad (47)$$

Since $\|y_{jz} - c_{iz}^{(a)}\|^2 \geq 0$, $\|\xi_{jz} - c_{iz}^{(a)}\|^2 \geq 0$, $\ln^2 \left(\sum_{e=1}^N \text{mean}(u_{ie}^{(a-1)}) + 1 \right) > 0$, and $m > 1$, it is known that Eq. (47) is positive. Therefore, Eq. (37) is a local minimum of Eq. (31).

Theorem 2. Let the membership matrix $u_{ij}^{(a)}$ and the weight matrix $w_{iz}^{(a)}$ be fixed, and the matrix $c_{iz}^{(a)}$ be a strict local minimum of Eq. (31) if and only if $c_{iz}^{(a)}$ is derived from Eq. (39).

Proof. Proving Theorem 2 is the same as proving Theorem 1. We only need to confirm that the second partial derivative of Eq. (31) for $c_{iz}^{(a)}$ is positive. For Eq. (48), the second partial derivative of Eq. (31) for $c_{iz}^{(a)}$ is positive. Therefore, Eq. (39) is also a local minimum of Eq. (31).

$$2 \sum_{j=1}^N \left(u_{ij}^{(a)} \right)^m \left(w_{iz}^{(a)} \right)^{\tau} \left(\frac{1}{\Delta y_{jz}} y_{jz} + \Delta y_{jz} \xi_{jz} \right) \quad (48)$$

Theorem 3. Let the membership matrix $u_{ij}^{(a)}$ and the center matrix $c_{iz}^{(a)}$ be fixed, and the matrix $w_{iz}^{(a)}$ be a strict local minimum of Eq. (31) if and only if $w_{iz}^{(a)}$ is derived from Eq. (46).

Proof. Here, we only need to prove that the second partial derivative of Eq. (31) for $w_{iz}^{(a)}$ is positive. The second partial derivative of Eq. (31) for $w_{iz}^{(a)}$ is:

$$\tau(\tau-1) \left(w_{iz}^{(a)} \right)^{\tau-2} \times \left[\sum_{j=1}^N \left(u_{ij}^{(a)} \right)^m \left(\left(\frac{1}{\Delta y_{jz}} \|y_{jz} - c_{iz}^{(a)}\|^2 + \Delta y_{jz} \|\xi_{jz} - c_{iz}^{(a)}\|^2 \right) \right) + \gamma \right] \quad (49)$$

Since $\|y_{jz} - c_{iz}^{(a)}\|^2 \geq 0$, $\|\xi_{jz} - c_{iz}^{(a)}\|^2 \geq 0$, $\gamma > 0$, and $\tau > 1$, it is known that Eq. (49) is positive. Therefore, Eq. (46) is a local minimum of Eq. (31).

4. Experiments and analysis

In this section, the noisy image segmentation experiments are comprehensively analyzed. The experimental results are compared with several FCM variants, including FCM (Peizhuang, 1983), FSC (Gan et al., 2006), FCM_NLS (Zhao et al., 2011), KWFLICM (Gong et al., 2012), ARKFCM (Elazab et al., 2015), ADFLICM (Zhang et al., 2017), FRFCM (Lei et al., 2018a), the fuzzy c-means clustering method based on feature-weight and cluster-weight learning (denoted as FCM_FWCW) (Hashemzadeh et al., 2019), SFFCM (Lei et al., 2018b), FCM_SICM

(Wang et al., 2020), CGFFCM (Oskouei et al., 2021). A brief description of the above algorithms is given here. FCM is the original algorithm. FSC assigns appropriate weights to each dimension of the image by introducing subspaces. FCM_NLS is a variant of FCM based on non-local spatial information. KWFLICM and ARKFCM are variants of FCM that incorporate kernel metrics. By defining a new spatial attraction model, ADFLICM has better segmentation performance for noisy images. FRFCM and SFFCM are two histogram-based FCM variant algorithms. FCM_FWCW and CGFFCM are feature weighting-based FCM variants algorithms that improve segmentation accuracy by setting weights for different clusters of clusters and pixel features. Finally, FCM_SICM combines local spatial information with intensity information and membership linking and segments noisy images.

4.1. Noise environment setting

In other papers, the test images were corrupted by only a single noise, and these methods showed superior performance. This paper adds mixed noise to all test images to test the technique in a natural environment. Here is the method of adding mixed noise:

Step1: Input image I .

Step2: Convert the data type of image I to ‘double’ and normalize it to between [0,1].

Step3: Set noise density ρ .

Step4: Contaminate image I with Gaussian noise with a mean value of zero and a variance of ρ .

Step5: Contaminate image I with salt & pepper noise with a density of ρ .

Step6: Contaminate image I with uniformly distributed multiplicative noise with a density of ρ .

Step7: Normalize the image I to [0,255] and convert the data type to ‘uint8’.

In the experiments followed, the mixed noise is described as $\rho \times 100\%$ mixed noise.

4.2. Setting of parameters

For the algorithm model, different parameter settings lead to various segmentation performances. Therefore, multiple parameters are selected in this section, and the set of parameters with the best segmentation results is chosen as the algorithm’s experimental parameters through several runs. For each method, the maximum iteration number $T = 100$, the minimum error $\eta' = 0.01$, and the membership weighting index $m = 2$. In FSC, the weight regularization parameter γ is set to 0.1. The local window radius l and the non-local window radius S of the non-local spatial information in FCM_NLS are set to 7 and 15, respectively, and the decay parameter g of the exponential function is set to 25. KWFLICM, ARKFCM, and ADFLICM are set with 5×5 neighborhood windows. A3 \times 3 structural element and a5 \times 5 local window are set for the morphological reconstruction operation of FRFCM. For FCM_FWCW and CGFFCM, p_{int} , p_{max} and p_{step} are set to 0, 0.5, and 0.01, respectively. For SFFCM, a minimum structure element of 3×3 is set for MMGR. The geometric and optical parameters σ_d and σ_r of FCM_SICM are set to 5 and 2.5, respectively.

For the proposed algorithm, the local window size $l = 7$, the non-local window radius $S = 15$, the decay parameter of the exponential function $g = 25$, the weight regularity parameter $\gamma = 0.7$, the fuzzy index $\tau = 2$, and the variance control parameter $\sigma = 500$. It is worth noting that references and heuristics set these parameters. For example, l , S , and h used for non-local space operations are mainly compared through the experimental results of (Zhao, 2013; Zhao et al., 2011; Wang et al., 2021), and the set of parameters with the best segmentation performance is selected as the experimental parameters. Heuristic methods calculated the membership weight index m and the fuzzy factor τ . The other parameters are determined experimentally.

4.3. Experiments on noisy grayscale images

Experiments on the segmentation of grayscale images containing noise are presented in this section, and detailed numerical results are given for 12 algorithms. Each input image is contaminated with 1%, 5%, 10%, and 15% of mixed noise. In this paper, we evaluate the performance of eleven algorithms and the proposed algorithm FSC_LNML with five evaluation metrics: Fuzzy Partition Coefficient (V_{PC}), Fuzzy Partition Entropy (V_{PE}), Segmentation Accuracy (SA), mean Intersection-over-Union (mIoU), and Normalized Mutual Information (NMI).

Fuzzy Partition Coefficient (V_{PC}) is an index for measuring the compactness of the membership degree:

$$V_{PC} = \frac{1}{N} \sum_{i=1}^k \sum_{j=1}^N u_{ij}^2 \times 100\% \quad (50)$$

The more significant V_{PC} , the better the segmentation result, and the more unique the attribution of each pixel to each cluster. V_{PC} is less than 100%. Fuzzy Partition Entropy (V_{PE}) is defined as:

$$V_{PE} = -\frac{1}{N} \sum_{i=1}^k \sum_{j=1}^N u_{ij} \ln(u_{ij}) \times 100\% \quad (51)$$

The smaller the V_{PE} , the better the partition effect. V_{PE} is greater than 0%. Segmentation Accuracy (SA) is the ratio of the total number of correctly segmented pixels to the total number of all pixels:

$$SA = \frac{\sum_{i=1}^k A_i \cap C_i}{\sum_{r=1}^k C_r} \times 100\% \quad (52)$$

where A_i is the i th pixel set in the segmentation result, and C_i is the i th pixel set in the ground-truth, the larger the SA, the better the segmentation performance. Average intersection-over-union (mIoU) is expressed as:

$$mIoU = \frac{1}{k} \sum_{i=1}^k \frac{A_i \cap C_i}{A_i \cup C_i} \quad (53)$$

All symbols are the same SA. It means that the segmented image is equal to the ground-truth value. Normalized mutual information (NMI) is defined as:

$$NMI = \frac{2MI(I_1, I_2)}{H(I_1) + H(I_2)} \times 100\% \quad (54)$$

where I_1 and I_2 are gray-scale images of equal size, $MI(I_1, I_2)$ represent the mutual information of I_1 and I_2 , $H(I_1)$ and $H(I_2)$ represent the entropy of I_1 and I_2 , respectively. The larger the NMI, the better the segmentation result.

The first experiment is to segment a noisy grayscale image 1 (Fig. 7(b): 256 \times 256 pixels) into two clusters, the second experiment is to segment the noisy grayscale image 2 (Fig. 8(b): 256 \times 256 pixels, pixel values of 0, 170, 255), and the third experiment was to segment the noisy grayscale image 3 (Fig. 9(b): 256 \times 256 pixels, four classes, pixel values of 0, 85, 170, 255). Figs. 7–9 and Tables 1–6 show the visual and numerical results, respectively.

For adequate analysis of the algorithm performance, this subsection is described in two parts, i.e., fuzzing reduction performance and segmentation performance.

Part 1: Fuzzing reduction performance.

V_{PC} and V_{PE} are two metrics to evaluate the fuzziness of membership. From Tables 1–2, we can see that the V_{PC} and V_{PE} of all algorithms decrease and increase with increasing noise, which indicates that, in general, the membership uncertainty is influenced by noise. The FCM_NLS algorithm performs better segmentation with a small noise density, mainly due to the better suppression of simple noise by non-local spatial information. And as the noise density increases, the algorithm’s performance gradually decreases, and the robustness decreases. Since the similarity metric in KWFLICM considers a local

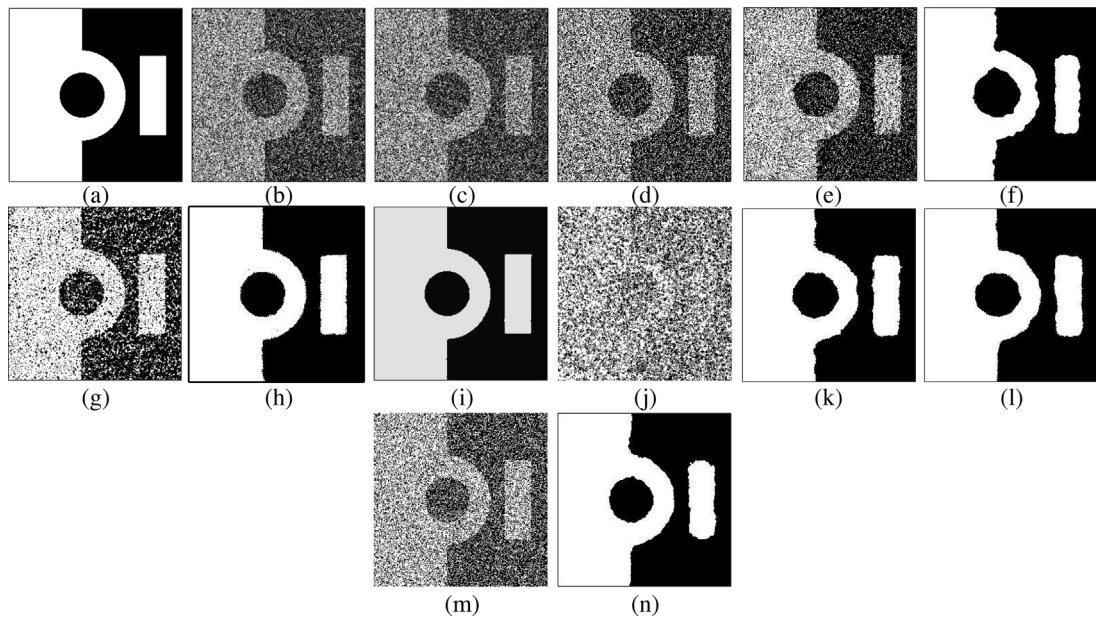


Fig. 7. Segmentation results of noisy grayscale image 1. (a) Original image. (b) Images contaminated with 30% mixed noise. (c) Result of FCM. (d) Result of FSC. (e) Result of FCM_NLS. (f) Result of KWFLICM. (g) Result of ARKFCM. (h) Result of ADFLICM. (i) Result of FRFCM. (j) Result of FCM_FWCW. (k) Result of SFFCM. (l) Result of FCM_SICM. (m) Result of CGFFCM. (n) Result of FSC_LNML.

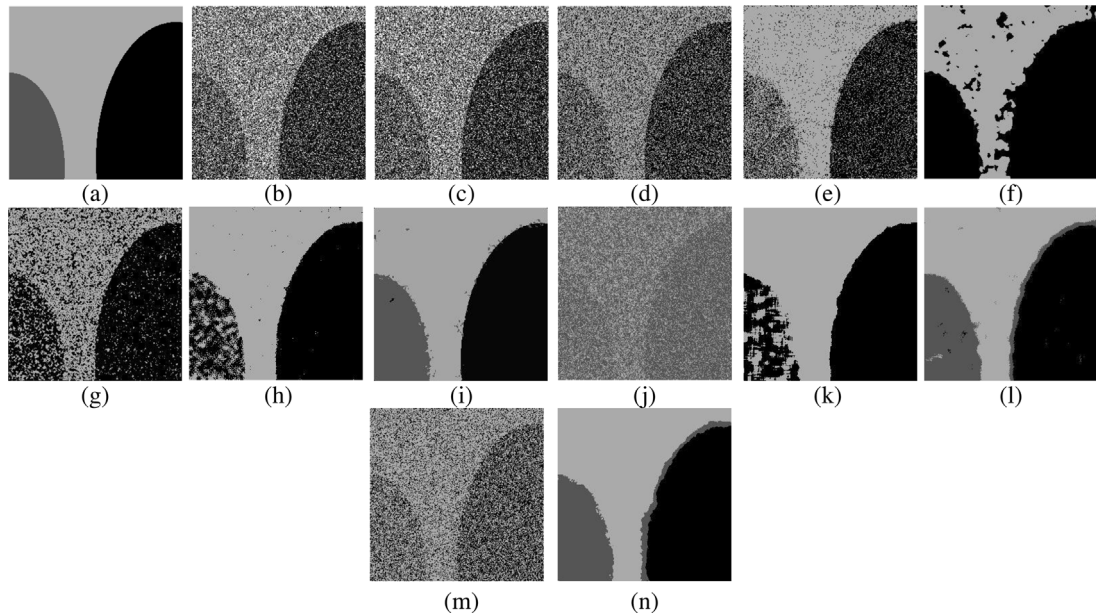


Fig. 8. Segmentation results of noisy grayscale image 2. (a) Original image. (b) Images contaminated with 30% mixed noise. (c) Result of FCM. (d) Result of FSC. (e) Result of FCM_NLS. (f) Result of KWFLICM. (g) Result of ARKFCM. (h) Result of ADFLICM. (i) Result of FRFCM. (j) Result of FCM_FWCW. (k) Result of SFFCM. (l) Result of FCM_SICM. (m) Result of CGFFCM. (n) Result of FSC_LNML.

membership template, which uses the idea of averaging membership values so that all membership values tend to be close to each other, this may increase the ambiguity of the segmentation. Compared to different comparative algorithms, the blurring of FCM_FWCW and CGFFCM are more severe, e.g., their mean values of V_{PC} are 57.94 and 64.65, respectively, which are lower than the original FCM algorithm. It is since both algorithms input the feature information of the image at the input rather than the image itself. However, when the image is severely corrupted by noise, these features are also corrupted, so the feature-based clustering is less capable of handling noisy images. However, FRFCM and FCM_SICM are better since all these algorithms use more complex spatial information extraction operations, making

the clustering results ambiguous. In all three experiments, the mean values of V_{PC} and V_{PE} of the proposed method FSC_LNML are 96.51% and 6.88%, respectively, and the variances are 3.73% and 6.18%, respectively. These results demonstrate that the method in this paper can segment the target better, reduce the ambiguity effect, and has better stability.

Part 2: Segmentation performance

Tables 3–5 show the segmentation quality of various algorithms under SA, mIoU, and NMI. In terms of segmentation metrics, the segmentation performance of FCM, FSC, FCM_FWCW, and CGFFCM is poor. The main reason is that FCM and FSC do not consider any spatial information of the image and therefore are less robust to noise. As

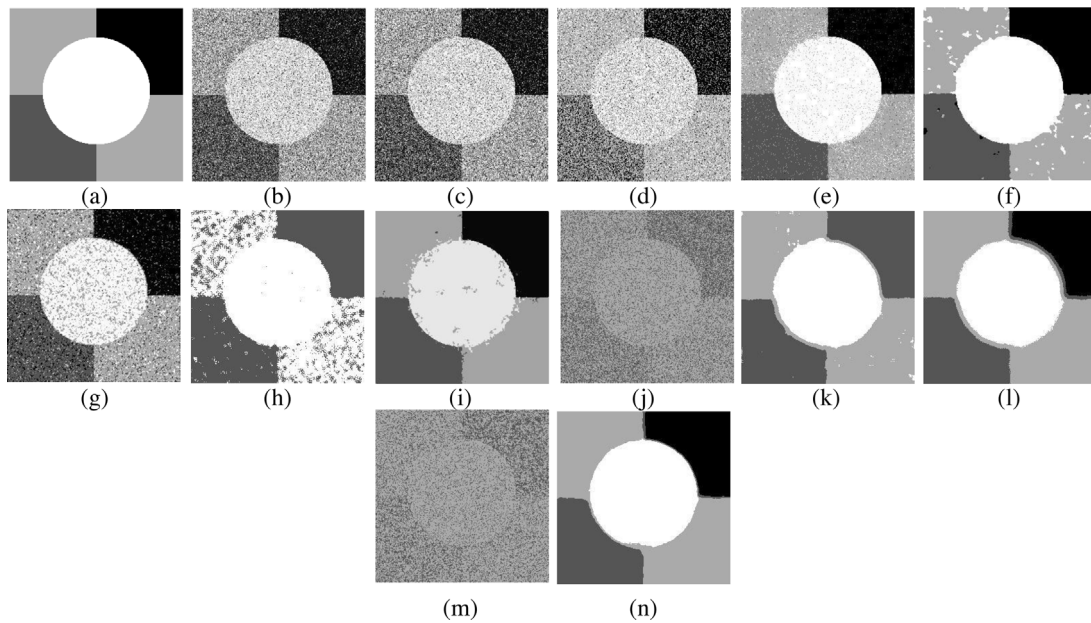


Fig. 9. Segmentation results of noisy grayscale image 3. (a) Original image. (b) Images contaminated with 30% mixed noise. (c) Result of FCM. (d) Result of FSC. (e) Result of FCM_NLS. (f) Result of KWFLICM. (g) Result of ARKFCM. (h) Result of ADFLICM. (i) Result of FRFCM. (j) Result of FCM_FWCW. (k) Result of SFFCM. (l) Result of FCM_SICM. (m) Result of CGFFCM. (n) Result of FSC_LNML.

shown in (c) and (d) in [Figs. 7–9](#), FCM and FSC almost fail to segment noisy images, and the results are full of noise. The FCM_FWCW and CGFFCM are featured vector-based clustering algorithms, i.e., when the algorithm performs clustering, the input is the features of the image rather than the image itself. And when the image is heavily contaminated with noise, the parts of the image are corrupted by the noise, resulting in the features input to the algorithm not representing the image information effectively, leading to mis-segmentation. As shown in (j) and (m) of [Figs. 7–9](#), the results of FCM_FWCW and CGFFCM are full of noise and have serious mis-segmentation. FCM_NLS shows better performance at low noise density, e.g., in segmenting grayscale images 2 and 3, the mIoU of FCM_NLS reaches 99.56% and 99.17%, which is higher than that of the proposed algorithm. However, the algorithm's performance decreases significantly as the noise density increases, mainly because the non-local space information has limited ability to suppress the high-density noise, and excessive preservation emerges, which makes the accuracy of the algorithm decrease. As shown in [Fig. 7\(e\)](#), when the noise density is 15%, there is a large amount of noise in the FCM_NLS results. Both KWFLICM and ADFLICM are variations of the FLICM-based algorithm, so the performance improves when processing noisy images, but there are also small noise patches in the results, as in [Fig. 8\(f\)](#), where the KWFLICM results retain a small amount of noise. In terms of visual effects, FRFCM, SFFCM, and FCM_SICM have better segmentation results. However, when segmenting grayscale image 2, SFFCM shows mis-segmentation, mainly because the uncertainty between pixels increases with the noise density, and the superpixel-based SFFCM does not perform well in handling the suspense, so the results are poor. The experimental results show that the numerical results of FRFCM and FCM_SICM are close to those of FSC_LNML. The reason is that FRFCM uses gradient reconstruction to preprocess the image and introduces membership filtering to smooth the membership values. In contrast, FCM_SICM extracts the spatial and intensity information of the image by bilateral filtering and uses the image itself for weight calculation, so the segmentation results are better. For the proposed method FSC_LNML, all three experiments have better SA, mIoU, and NMI, and their mean values reach 99.55%, 98.06%, and 97.10%, respectively, and the variance reaches 0.63%, 1.80%, and

1.71%, respectively. The experiments show that the proposed method FSC_LNML can better solve the noisy image segmentation problem with good stability performance under local variance information, non-local spatial information, and adaptive constraints. The iteration step number is also an important indicator to evaluate the algorithm's performance. The number of iteration steps used for convergence of the objective function of various algorithms is given in [Table 6](#), from which it is known that the number of iteration steps generally increases with the aggravation of the mixing noise. Among all the compared algorithms, KWFLICM has giant iteration steps, generally above 100. Since FCM_SICM introduces membership linking in the denominator of the objective function, it makes the value of the objective function decrease, and therefore effectively reduces the number of iteration steps. The proposed method FSC_LNML presents the mean membership linking, which solves the problem that the algorithm converges before reaching the optimum, and therefore the number of iteration steps is less.

4.4. Experiments on noisy color images

The numerical results in the previous section demonstrate that FSC_LNML is a suitable method for noisy grayscale image segmentation. Five experiments are performed on different color image databases in this section. The first experiment segmented six color images gathered from the BSDS500 database ([Arbelaez et al., 2010](#)) created by the Berkeley Computer Vision Group. From left to right in [Fig. 10](#), the images are contaminated with 10%, 5%, 15%, 5%, 20%, and 30% of mixed noise, respectively. High contrast colors were applied to distinguish segmented areas, especially in the results filled with noisy pixels.

From [Fig. 10](#), the results of FCM and FSC are filled with noisy pixels, and the segmentation objectives are hard to identify, indicating that these algorithms are sensitive to noise. The segmentation results of FCM_NLS for #3063, #42049, and #100007 are well and could segment the target, yet the segmentation results in other images are full of noise, resulting in poor visual effects. It indicates that the non-local spatial information is less stable during segments for color images. The

Table 1Comparison of V_{PC} (%) of twelve methods on three grayscale images corrupted by different mixed noise.

Image	Noise	FCM	FSC	FCM_NLS	KWFLICM	ARKFCM	ADFLICM	FRFCM	FCM_FWCW	SFFCM	FCM_SICM	CGFFCM	FSC_LNML
Synthetic image 1	1%	98.55	98.53	99.61	95.18	99.35	92.13	88.46	76.72	98.24	96.35	82.33	99.34
	5%	92.50	92.40	97.71	94.50	96.13	90.05	88.35	70.44	96.63	95.80	85.94	99.25
	10%	89.13	88.99	94.23	93.84	63.88	85.43	88.28	68.53	92.45	95.11	76.73	99.03
	15%	88.65	88.75	90.01	91.56	89.23	80.66	88.12	60.09	85.89	94.45	70.22	98.57
Synthetic image 2	1%	83.18	83.34	95.92	92.03	70.80	90.05	66.71	62.88	62.20	93.83	65.84	99.06
	5%	82.34	82.50	83.50	78.55	82.45	88.74	66.46	54.53	54.52	90.39	65.21	98.03
	10%	83.95	84.05	73.17	78.30	76.14	88.20	66.24	55.26	45.97	86.19	63.72	96.02
	15%	85.52	85.46	71.21	76.71	73.71	85.44	66.69	50.89	39.46	81.52	61.09	93.27
Synthetic image3	1%	80.91	80.82	93.63	68.87	76.70	53.52	54.32	50.34	44.03	98.77	53.43	98.52
	5%	81.06	80.92	75.89	65.09	77.04	54.83	53.65	49.43	40.56	83.59	52.18	96.35
	10%	81.91	82.01	65.36	48.29	71.98	52.29	53.03	48.52	35.81	63.28	50.69	92.50
	15%	83.84	84.00	60.78	43.58	70.63	50.88	54.46	47.69	31.78	70.78	48.42	88.13
Mean		85.96	85.98	83.42	77.21	79.00	76.01	69.56	57.94	60.63	86.81	64.65	96.51
Variance		5.12	5.09	13.03	17.10	10.35	16.61	14.23	9.32	24.48	10.10	11.89	3.37

Table 2Comparison of V_{PE} (%) of twelve methods on three grayscale images corrupted by different mixed noise.

Image	Noise	FCM	FSC	FCM_NLS	KWFLICM	ARKFCM	ADFLICM	FRFCM	FCM_FWCW	SFFCM	FCM_SICM	CGFFCM	FSC_LNML
Synthetic image 1	1%	3.64	3.67	1.02	9.84	1.62	24.38	22.48	43.45	3.15	6.66	38.55	1.07
	5%	13.70	13.89	5.00	11.08	7.76	25.84	22.59	46.89	6.87	8.20	40.23	1.33
	10%	18.64	18.83	11.01	12.25	52.56	29.69	22.68	47.52	15.30	9.91	33.21	1.94
	15%	19.41	19.22	17.62	16.43	18.78	36.73	22.92	49.98	26.17	11.21	52.15	2.53
Synthetic image 2	1%	30.68	30.40	9.62	18.06	50.88	64.83	61.46	67.84	62.77	14.12	65.62	2.08
	5%	32.43	32.21	31.39	41.13	32.04	65.62	61.66	62.15	75.23	21.35	64.28	4.78
	10%	29.56	29.41	47.90	42.18	42.13	69.99	62.04	70.77	89.65	29.23	67.82	9.08
	15%	26.71	26.81	51.68	44.45	46.08	73.28	61.51	71.84	100.20	37.19	70.44	14.29
Synthetic image3	1%	37.13	37.30	14.99	61.24	45.77	89.84	87.90	92.22	90.82	21.90	85.43	3.36
	5%	36.61	36.86	46.62	69.85	42.93	88.73	89.01	94.37	105.46	35.17	87.62	6.39
	10%	34.78	34.58	64.91	98.59	52.09	90.02	90.06	90.09	115.68	71.01	89.27	16.29
	15%	31.13	30.84	73.42	106.69	54.71	91.94	87.73	89.87	124.15	57.24	85.43	19.37
Mean		26.20	26.17	31.26	44.31	37.28	62.57	57.67	68.91	67.95	26.93	65.00	6.88
Variance		9.85	9.81	23.76	32.37	17.46	25.46	27.10	18.45	42.24	19.49	19.28	6.14

Table 3

Comparison of SA (%) of twelve methods on three grayscale images corrupted by different mixed noise.

Image	Noise	FCM	FSC	FCM_NLS	KWFLICM	ARKFCM	ADFLICM	FRFCM	FCM_FWCW	SFFCM	FCM_SICM	CGFFCM	FSC_LNML
Synthetic image 1	1%	54.01	99.79	99.71	99.91	99.83	99.74	99.96	85.43	99.94	99.87	86.85	99.21
	5%	54.01	97.87	99.64	99.87	99.60	99.21	99.96	84.34	99.90	99.85	84.52	99.98
	10%	54.01	94.88	99.85	99.87	73.64	98.52	99.51	80.26	99.80	99.87	83.24	99.95
	15%	54.01	92.98	98.18	99.91	97.07	99.20	99.94	84.21	99.79	99.79	83.37	99.60
Synthetic image 2	1%	14.51	99.17	99.84	99.44	99.82	99.43	99.78	83.52	97.09	98.63	86.27	99.91
	5%	31.84	85.22	98.41	85.26	95.58	99.20	99.77	81.09	99.40	98.37	85.19	99.80
	10%	34.58	82.51	86.81	99.32	95.28	98.72	99.39	80.88	99.75	98.47	84.43	99.76
	15%	35.92	81.05	86.05	99.87	79.36	88.74	99.80	79.64	99.48	98.53	82.00	99.27
Synthetic image3	1%	62.15	93.97	99.84	98.90	99.71	98.43	99.47	82.11	98.56	98.25	85.37	99.99
	5%	47.98	75.25	95.30	97.28	93.32	98.52	99.00	80.25	81.13	98.09	84.59	99.46
	10%	61.22	61.34	86.17	80.19	90.00	97.66	98.50	78.84	77.37	81.85	83.62	99.27
	15%	61.53	72.60	76.56	75.66	87.59	90.09	99.56	76.52	87.07	97.36	80.88	97.65
Mean		47.15	86.39	93.86	94.62	92.57	97.28	99.55	81.42	94.94	97.41	84.19	99.55
Variance		14.15	11.67	7.56	8.49	8.20	3.57	0.42	2.48	7.85	4.76	1.62	0.63

KWFLICM algorithm segmented #24063 into scattered block regions, while a small number of noise patches appeared in the segmentation results of #86016, indicating that the kernel metric-based method is also less robust on some occasions. The results of ARKFCM and ADFLICM are also full of noise, meaning that this class of algorithms has a limited ability to suppress noise. The FCM_FWCW and CGFFCM algorithms show severe mis-segmentation and almost fail to segment the target, indicating that this class of algorithms cannot better segment noisy images. Since FRFCM and SFFCM are gradient reconstructions and superpixel-based clustering algorithms, these methods are less capable of handling uncertainty. Therefore, these two algorithms cannot correctly identify the boundaries of segmented targets, leading to mis-segmentation. For example, SFFCM can hardly segment the target with severe information loss, while FRFCM has poor noise suppression and severe mis-segmentation. In all experiments, the algorithm FSC_LNML

in this paper suppresses the noisy pixels and segments the region with high accuracy.

4.4.1. Experiments with noisy remote sensing images

The second experiment segments six color remote sensing images gathered from the AID (Xia et al., 2017) database, containing 30 categories. Images of farmland, ponds, rivers, and squares are selected here. Each image is 600 × 600 pixels in size, and each image is contaminated with 15% mixed noise.

In Fig. 11, the result of each segmentation is clear and can be better suppressed by noise. Different types of farmland and land boundaries can be better distinguished in the first column. Along with the second and third columns, there are no noisy pixels in the segmentation results of the pond image, and the pond target and the surrounding wasteland can be identified more accurately. Along with the fourth and fifth

Table 4

Comparison of mIoU (%) of twelve methods on three grayscale images corrupted by different mixed noise.

Image	Noise	FCM	FSC	FCM_NLS	KWFICM	ARKFCM	ADFLICM	FRFCM	FCM_FWCW	SFFCM	FCM_SICM	CGFFCM	FSC_LNML
Synthetic image 1	1%	25.23	99.03	99.42	49.47	99.17	98.42	99.83	88.94	99.70	99.50	88.00	99.99
	5%	45.99	90.84	99.26	49.39	97.19	97.69	99.83	82.19	99.54	99.44	70.98	99.91
	10%	45.99	75.63	99.29	49.25	54.90	96.55	98.95	70.66	99.27	99.37	68.54	99.80
	15%	45.99	63.42	92.98	47.86	88.54	90.03	99.81	71.29	98.88	98.94	66.43	99.04
Synthetic image 2	1%	72.69	73.38	99.56	33.12	71.89	97.43	98.37	75.52	94.06	95.09	79.82	98.49
	5%	66.67	60.86	92.84	23.92	76.58	96.88	98.31	73.43	76.03	94.71	78.43	98.54
	10%	65.17	51.35	68.64	25.43	61.30	95.12	97.75	72.29	81.27	94.48	76.00	98.16
	15%	65.71	45.84	64.51	23.20	47.04	90.09	96.14	70.00	85.23	94.15	71.37	98.52
Synthetic image3	1%	17.65	75.36	99.17	13.41	51.51	96.84	94.30	63.59	93.79	93.03	74.47	97.75
	5%	31.48	38.23	86.56	23.46	65.47	95.43	95.33	65.84	66.69	91.70	72.15	97.28
	10%	30.57	27.01	54.89	12.15	46.55	90.02	94.42	61.77	61.64	66.32	68.01	95.86
	15%	31.94	21.69	41.18	13.72	38.46	88.74	94.47	60.52	54.76	90.58	66.52	93.39
Mean		45.42	60.22	83.19	30.36	66.55	94.43	97.29	71.33	84.24	93.11	73.39	98.06
Variance		17.73	23.18	19.65	14.31	19.53	3.45	2.14	7.91	15.45	8.61	6.10	1.80

Table 5

Comparison of NMI (%) of twelve methods on three grayscale images corrupted by different mixed noise.

Image	Noise	FCM	FSC	FCM_NLS	KWFICM	ARKFCM	ADFLICM	FRFCM	FCM_FWCW	SFFCM	FCM_SICM	CGFFCM	FSC_LNML
Synthetic image 1	1%	95.67	95.54	97.37	95.37	96.10	97.62	98.99	65.53	98.37	97.47	70.18	99.91
	5%	72.20	72.16	96.75	94.73	89.39	95.43	99.02	63.28	97.66	97.19	68.74	99.44
	10%	43.00	42.39	96.59	93.83	17.87	92.20	95.55	60.09	96.48	96.92	66.43	98.83
	15%	24.88	24.70	77.38	86.39	66.84	88.74	98.92	54.23	94.99	95.22	60.99	95.74
Synthetic image 2	1%	77.78	78.01	96.61	97.76	49.24	88.82	97.70	58.34	88.12	90.86	63.65	98.41
	5%	39.00	39.07	91.38	88.88	65.75	87.68	98.66	59.29	59.67	90.06	60.09	96.61
	10%	10.04	21.27	59.66	56.82	39.27	81.29	96.50	55.43	66.57	90.48	58.43	98.22
	15%	6.75	13.41	44.26	46.60	19.02	80.52	98.89	50.58	69.53	90.44	54.12	94.43
Synthetic image3	1%	73.12	72.23	99.53	35.09	34.92	85.43	96.13	52.38	92.34	92.59	55.57	96.11
	5%	32.05	30.84	86.56	95.06	64.27	84.98	95.59	54.65	90.14	91.16	52.19	95.83
	10%	17.49	19.92	57.09	72.89	42.58	78.89	95.20	50.21	87.33	88.89	56.84	95.24
	15%	10.35	13.41	46.04	74.70	31.30	77.64	93.08	49.83	81.49	90.87	54.37	96.39
Mean		41.86	43.58	79.10	78.18	51.38	86.60	97.02	56.15	85.22	92.68	60.13	97.10
Variance		29.31	27.30	20.52	20.44	24.37	6.12	1.87	4.96	12.58	3.00	5.73	1.71

Table 6

Comparison number of iteration steps of twelve methods on three grayscale images corrupted by different mixed noise.

Image	Noise	FCM	FSC	FCM_NLS	KWFICM	ARKFCM	ADFLICM	FRFCM	FCM_FWCW	SFFCM	FCM_SICM	CGFFCM	FSC_LNML
Synthetic image 1	1%	24	40	55	>100	30	39	19	66	22	10	66	7
	5%	25	41	59	>100	34	42	22	69	36	18	65	10
	10%	30	45	60	>100	25	44	25	75	36	22	66	13
	15%	35	55	66	>100	28	42	32	70	50	13	63	14
Synthetic image 2	1%	24	27	20	>100	25	38	18	58	29	13	55	11
	5%	26	27	23	>100	37	38	16	54	34	9	57	28
	10%	33	37	29	>100	40	37	22	53	44	11	56	29
	15%	35	38	38	>100	42	42	22	52	43	14	57	30
Synthetic image3	1%	25	36	40	>100	17	25	18	59	33	12	63	9
	5%	39	40	35	>100	19	22	20	58	43	10	60	9
	10%	42	45	45	>100	25	23	24	54	40	15	64	13
	15%	44	53	53	>100	23	27	26	43	42	22	63	21

columns, the rivers are well-segmented, and the edges of the river bends are well maintained. The green area of the square image and the road are segmented well in the last column, with few noisy pixels. In summary, the proposed method FSC_LNML has higher accuracy and robustness for noisy remote sensing image segmentation.

4.4.2. Results of color image segmentation with noise from MSRC database

The third experiment is the segmentation of six color images gathered from the MSRC ([Shotton et al., 2006](#)). The MSRC dataset contains 23 object classes, including 591 natural images. The images of the building, cow, chimney, bird, and sign were collected here. Each image is 640 × 480 pixels in size, and each image is contaminated with 10% mixed noise.

In [Fig. 12](#), the results of each segmentation are precise and allow for better noise suppression. The target and background can be well distinguished in the first and fifth columns, and there are fewer noisy pixels in the results. In the second column, due to the color of the

cow and the grass's color being too similar, it makes them into one category, but the main target in the image is better segmented. The segmentation results are evident in the third, fourth, and last columns with few noisy pixels. In conclusion, the proposed method FSC_LNML has higher accuracy and robustness for performing different types of noisy image segmentation.

4.4.3. Results of MR image segmentation with noise

The fourth experiment segments twelve MR images with noise gathered from three different databases. It is well known that MR images involve much detail, which is crucial for medical diagnosis. Therefore, non-local spatial information was used in a 7×7 ($S = 7$) region, avoiding excessive smoothing of details. The brain MR image in the first column in [Fig. 13](#) was collected from the open-access database,¹ and had

¹ <http://www.med.harvard.edu/aanlib/home.html>.

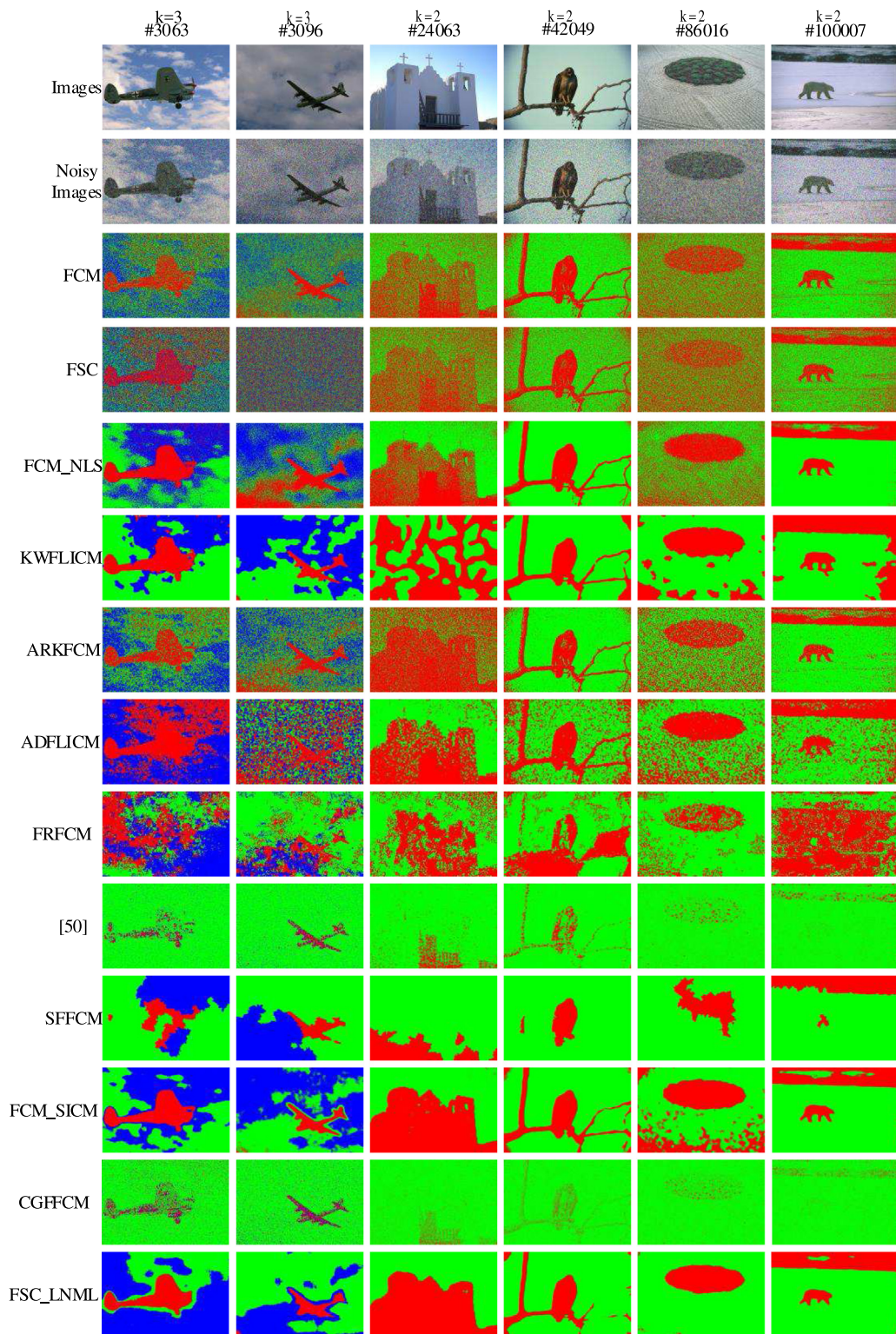


Fig. 10. Results of segmentation of six color images collected in the BSDS500 database by twelve algorithms.

256 × 256 pixels. The brain MR images in the second to sixth columns were collected from the SBD (Simulated Brain Database) ([Cocosco et al., 1997](#)) where the second column has 181 × 217 pixels, the third and fourth columns have 217 × 181 pixels, and the fifth and sixth columns have 240 × 240 pixels. The knee MR images in [Fig. 14](#) were

collected from the open-access database.² and have 350 × 350 pixels. Each image is contaminated by 5% mixing noise.

It can be seen that for all segmentation results, the MR images have almost no noisy pixels. For the segmentation results in the third to sixth

² <https://www.mr-tip.com/serv1.php?type=img&img=Knee%20MRI%20Sagittal%20T1%200001>.

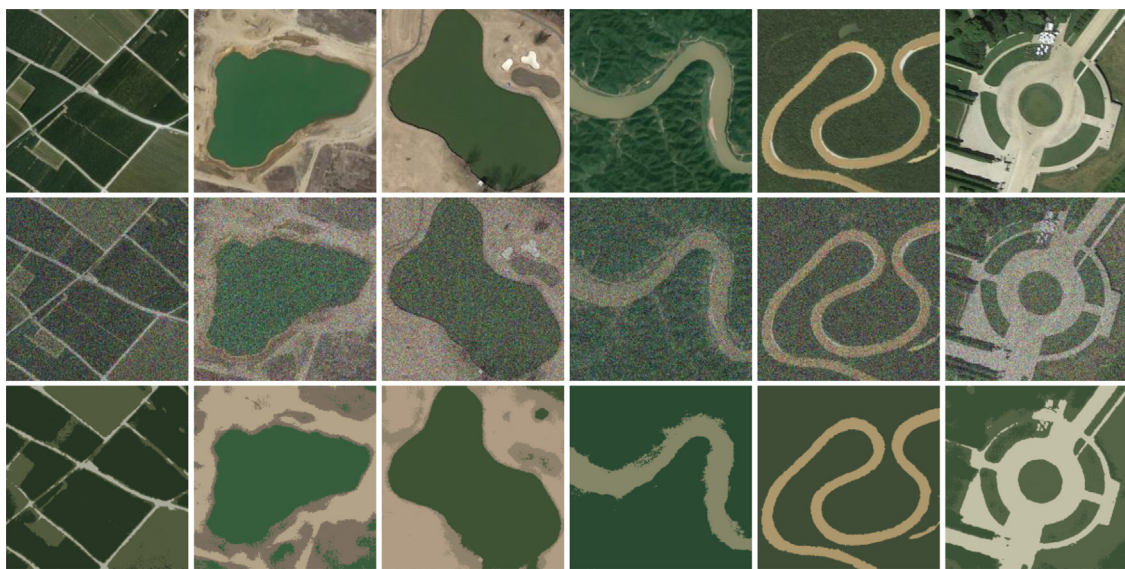


Fig. 11. Results of segmentation of six remote sensing images collected in the AID database using the proposed method.

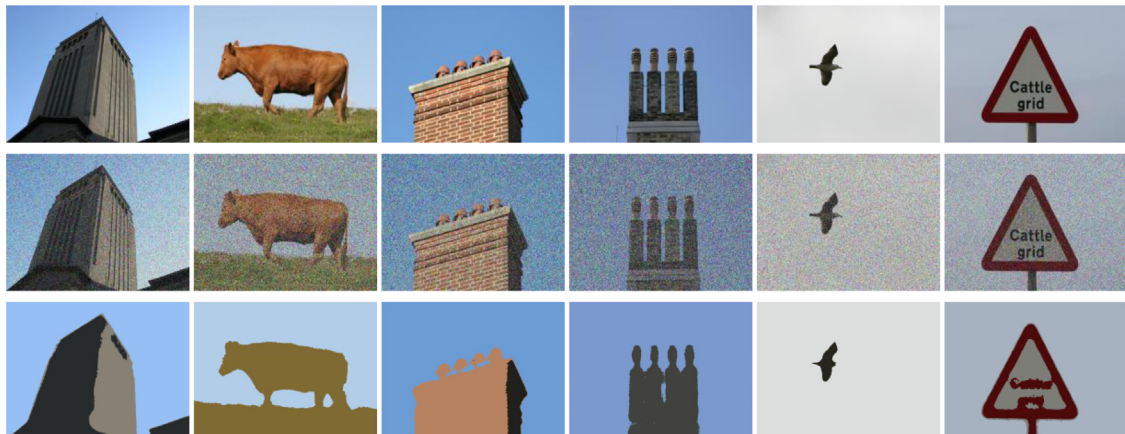


Fig. 12. Results of segmentation of six color images collected in the MSRC database using the proposed method.

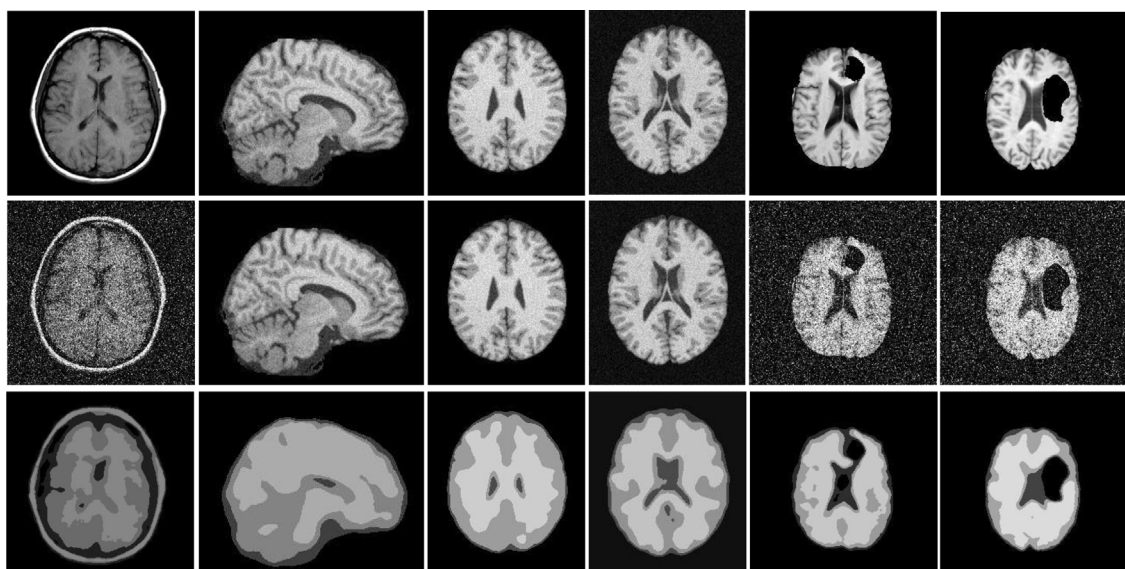


Fig. 13. The results of segmentation of six brain MR images collected in different databases using the proposed method.

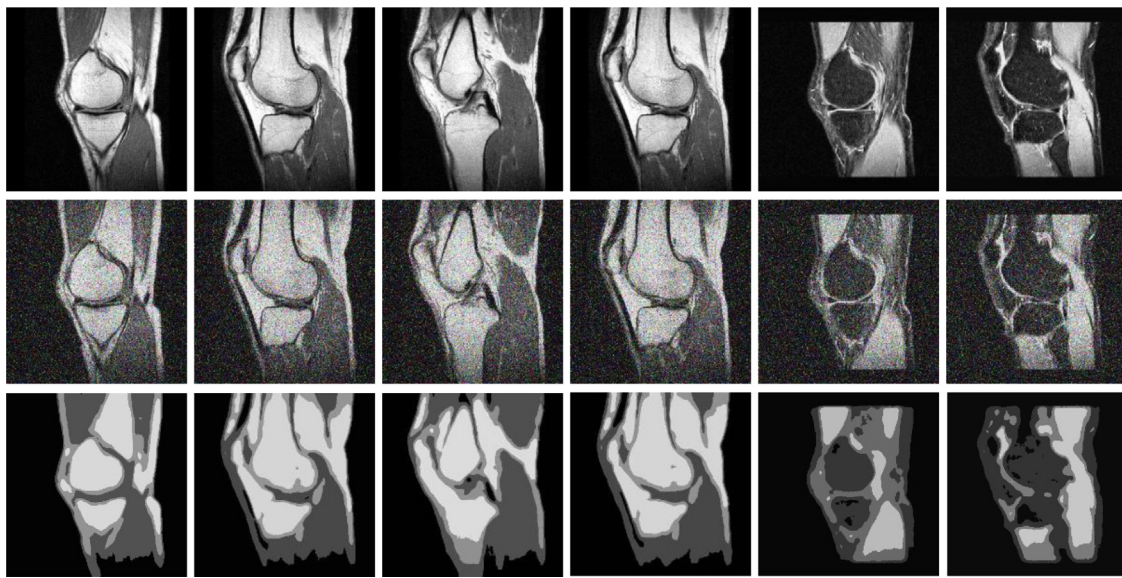


Fig. 14. The result of segmentation of six knee MR images collected in a public database using the proposed method.

columns in Fig. 13, the white and gray matter structures are segmented well. It is worth noting that the details of the black area in the center of the segmentation result are preserved. However, one drawback is that some small details are incorrectly segmented when splitting the first and second columns. For example, in the first column of the segmented result, the black region in the middle is incorrectly segmented into gray matter structures, and the boundary of the brain sulcus in the second column is partially missing, indicating that the algorithm in this paper has poor segmentation ability for small image targets. For the segmentation results in Fig. 14, the segmentation results are still apparent, and the whole structure of the bone is segmented well. However, due to the gradual change of grayscale, the region at the bottom of the segmentation result is incorrectly segmented as a black background, which indicates the limitation of the proposed method FSC_LNML in handling grayscale gradients. Overall, the proposed method FSC_LNML can segment noisy MR images.

4.4.4. Results of common color image segmentation with noise

Finally, six common noisy color images were segmented, and all images were corrupted by 15% of mixed noise. The dimensions of these six images are 500×306 pixels, 500×333 pixels, 451×354 pixels, 448×270 pixels, 600×600 pixels, and 300×219 pixels, respectively. The segmentation results of the proposed method FCM_LNML in this paper are shown in Fig. 15.

We can see that all segmentation results have no noisy pixels, and the segmented regions are smoother and have better edge fit, which indicates that the proposed method FSC_LNML has good noise suppression and edge-preserving ability.

The above experiments are summarized as follows: (1) The proposed algorithm utilizes local variance & non-local spatial information to mine the knowledge of the image to improve the robustness of the algorithm. The difference between the original image and the local variance & non-local spatial information is adaptively constrained to the objective function without artificially setting the constraint parameters, which avoids the interference of uncertainties and further improves the algorithm's robustness. The mean membership linking was exploited to reduce the number of iterations of the algorithm, while the segmentation performance of color images was improved by introducing subspaces. Therefore, these better segmentation results result from the algorithm taking full advantage of its information rather than being generated by overfitting. (2) Experiments with grayscale images and different color images show that the proposed algorithm can handle

noisy images in various settings, and it also shows that the algorithm has a good generalization capability. Therefore, the proposed algorithm could be applied to general color image segmentation, remote sensing image classification, and medical segmentation. For example, during fire detection, it is difficult to analyze the extent of fire spread with general image segmentation algorithms due to the blurring of the edges of the fire region caused by the burning of flames. The proposed algorithm introduces the fuzzy theory, which can better deal with the uncertainty problem and has better robustness in the face of other disturbing factors such as noise. Then, in remote sensing engineering applications, the edge contours of remote sensing images are blurred, and the proposed algorithm can be utilized to better segment the noisy remote sensing images. Another example is that MR images are essential for diagnosing brain diseases in medical image applications. Brain MR images are easily disturbed by noise during acquisition, making the images blurred and affecting the doctors' diagnosis. The proposed algorithm may be employed to better segment the noisy MR images. (3) It is possible to combine the current work with nonlinear systems to deal with some ideas about nonlinear models (Albu et al., 2019; Janmaiaya et al., 2021). For example, we can combine the current work with fuzzy signature (Wong et al., 2004) and expert system (Pozna and Precup, 2014) to build MRI pre-clinical diagnosis system. As mentioned before, MR images are susceptible to the interference of noise during acquisition, which makes the images blurred or some data lost. The proposed algorithm can better suppress the noise, while the fuzzy signature can better deal with the data blurring and loss, so the current work and fuzzy signature can be combined to build an expert system for MRI pre-clinical diagnosis.

4.5. Investigation of parameter sensitivity

For FSC_LNML, the weight regularization parameter γ and the variance control parameter σ are essential. The results of V_{PC} , V_{PE} , SA, mIoU, NMI, and iteration steps affected by mixed noise in Fig. 9(b) are shown in Fig. 16. From Fig. 16, it can be seen that the values of V_{PC} , SA, mIoU, and NMI increase as γ increases, while V_{PE} and iteration steps are decreasing. After γ is 0.7, the growth rate of each index gradually tends to smooth out, so this paper sets $\gamma = 0.7$. Then we analyze the effect of σ on the performance indexes. When σ increases, the performance index increases, and the index reaches the highest when $\sigma = 500$, so $\sigma = 500$ is set in this paper.

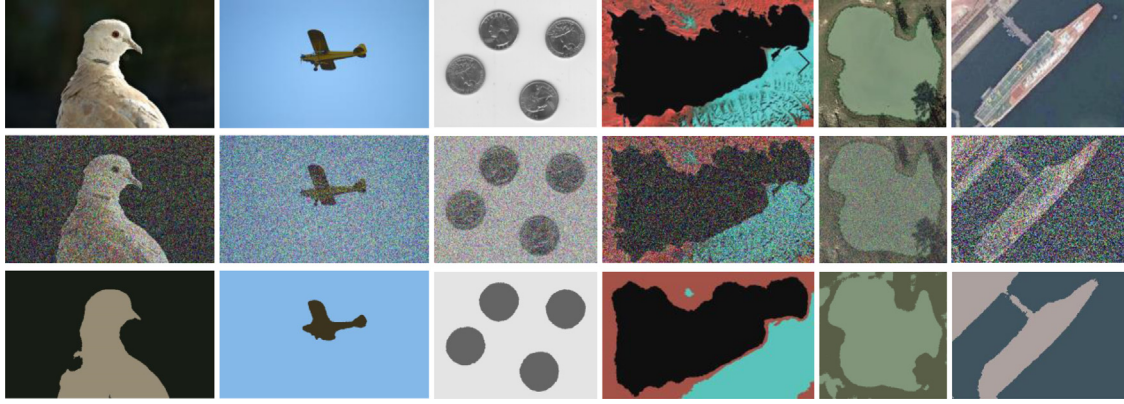
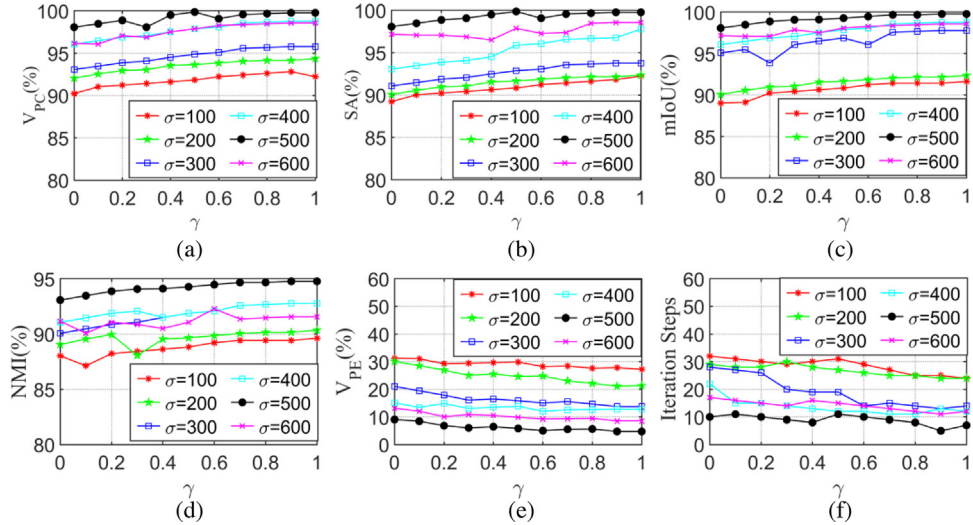


Fig. 15. Results of segmentation of six common color images using the proposed method.

Fig. 16. The effects of different γ and σ on segmentation performance.

4.6. Analysis of computational complexity

Computational complexity is an essential factor in evaluating methods. In general, the same computational complexity is challenging to obtain. The number of computational steps to calculate the objective function in the clustering process is calculated. The calculation process is as follows. Firstly, the calculation step expression E of the objective function is calculated. Secondly, all variables E are unified n to obtain the calculation step function $E(n)$. Finally, n is set to infinity. Find an auxiliary function $f(n)$, so that $f(n)/E(n) = a$ is true, then $f(n)$ and $E(n)$ are of the same order of magnitude, $O[f(n)]$ is the time complexity, where a is constantly greater than 0.

In Table 7, N is the number of pixels in the image, k are the number of clusters, T is the number of iterations, h is the side length of the local neighborhood, M is the number of features, Q is the number of pixels, S and l are respectively the local window and non-local window side length. T_M and T_W are the numbers of calculation steps for the MMGR-WT and watershed methods, respectively. P is the number of superpixels. It is worth noting that among the various algorithms, KWFLICM has the highest complexity. Because KWFLICM needs to calculate the fuzzy weight factor before clustering, the computational complexity is $O(n^7)$. The proposed FSC_LNML is similar to FCM_NLS, which uses non-local information to obtain image spatial data, so the complexity is $O(n^5)$. The algorithm in this paper is different from KWFLICM in that the local variance template is calculated in advance to reduce the complexity.

5. Discussion

The advantages and disadvantages of other methods and the proposed method FSC_LNML are discussed in this section. Firstly, the local information-based FCM algorithm has been widely applied and claimed to have good robustness. However, noise may exist in the local pixel window as the noise density is high, so the local information-based FCM algorithm has limited ability to suppress high-density noise. Bias field correction is often employed to deal with grayscale inhomogeneity (Mishra et al., 2020), and the combination of local information and bias field correction algorithms are widely utilized in segmenting brain MR images. Nevertheless, this type of algorithm fails to segment noisy images better due to the limited ability of local information to suppress noise. Secondly, the histogram-based FCM algorithm is high-speed because the image's gray level is much smaller than the number of pixels. FSC_LNML cannot achieve this advantage, so the artificial bee colony algorithm (Hasheminejad and Vosoughian, 2020) can be considered to speed up the algorithm's convergence and reduce the algorithm running time. Thirdly, since the hidden Markov random field considers the previous state of the current affiliation, it can extract the contextual information of local pixel blocks and obtain better results than FCM in image segmentation. Nevertheless, noise could corrupt the contextual knowledge of the image, resulting in a local region that may contain too many noisy pixels, thus reducing the segmentation accuracy. Fourthly, the non-local information is more capable of denoising,

Table 7
Complexity overloads of twelve methods.

Segmentation algorithm	Calculation step E	Calculation step function $E(n)$	Time complexity
FCM	$N \times k \times T$	n^3	$O(n^3)$
FSC	$N \times k \times T$	n^3	$O(n^3)$
FCM_NLS	$N \times (2S+1)^2 \times (2l+1)^2 + N \times k \times T$	$n^5 + n^3$	$O(n^5)$
KWFLICM	$N \times [(2h^2)^2 + 5h^2] \times k \times T$	n^7	$O(n^7)$
ARKFCM	$N \times [2h^2 + (h^2 - 1) + 1] + N \times k \times T$	$n^3 + n^3$	$O(n^3)$
ADFLICM	$N \times h^2 \times k \times T$	n^5	$O(n^5)$
FRFCM	$N \times h^2 + Q \times k \times T$	$n^3 + n^3$	$O(n^3)$
FCM_FWCW	$T \times (NMK + NMK + NMK + NMK)$	n^4	$O(n^4)$
SFFCM	$N \times h^2 + T_M + P \times k \times T$	$n^3 + n^2 + n^3$	$O(n^3)$
FCM_SICM	$N \times Q \times \log_2(H \times W \times Q) + N + N \times k \times T$	$n^3 + n + n^3$	$O(n^3)$
CGFFCM	$T \times (NMK + NMK + NMK + NMK)$	n^4	$O(n^4)$
FSC_LNML	$N \times (2S+1)^2 \times (2l+1)^2 + N \times (2n+1)^2 + N \times k \times T$	$n^5 + n^3 + n^3$	$O(n^5)$

yet the apparent drawback is the high time complexity, then the computational efficiency of the proposed FSC_LNML is limited. On the other hand, since the non-local information utilizes the average value of the distance between dimensions for each color pixel, it indicates that the data of each dimension is processed equally. However, in clustering, the impact of pixels between different sizes may be unequal. The proposed FSC_LNML utilizes subspace to assign appropriate weights to each image dimension to improve the segmentation performance of color images. Finally, the kernel approach allows the data to be mapped nonlinearly to higher dimensions, so the FCM variant that takes the kernel function approach enables data clustering with complex shapes. Nevertheless, the kernel metric-based approach can lead to memory overflow while dealing with extensive data, so the FCM algorithm can be considered to be combined with other clustering algorithms to form a unified form of clustering algorithm (Borlea et al., 2021) to overcome the hardware limitations that may occur when dealing with extensive data. In contrast, the proposed FSC_LNML utilizes the Euclidean distance, more practical for spherical data.

6. Conclusion

Many FCM variables are proposed to deal with the uncertainty of noisy image segmentation. Non-local spatial information and membership linking are two better methods to enhance the robustness of FCM and reduce the number of iteration steps. However, as the noise density increases, there is under-segmentation of non-local spatial information, while the membership linking will have more outliers, which will cause the algorithm to converge prematurely when the result is not optimal. Many algorithms utilize the average value of the distance between each dimension for each color pixel, indicating that the processing of each dimension data is equal. Nevertheless, in clustering, the influence of pixels between different dimensions may not be equal. This paper introduces new ideas to solve the above three issues and proposes an improved fuzzy subspace clustering with adaptive local variance & non-local spatial information and mean membership linking. Firstly, a local variance template is proposed to overcome the under-segmentation of non-local spatial information and integrate local variance & non-local spatial information into the objective function of FCM to enhance robustness. Secondly, the mean membership linking is utilized as the denominator of the objective function to reduce the number of iterations and prevent the objective function from converging before reaching the optimum. Thirdly, the absolute intensity difference between the original image and the local variance & non-local spatial information is used to constrain the original image and the local variance & non-local spatial information. Finally, improve the segmentation performance of color images by allocating appropriate weights to each dimension based on subspace. Experiments are implemented using FCM, FSC, FCM_NLS, KWFLICM, ARKFCM, ADFLICM, FRFCM, FCM_FWCW, SFFCM, FCM_SICM, CGFFCM, and the proposed FSC_LNML under mixed noise. The results show that when the image is severely damaged by noise, the proposed FCM_LNML has the best performance and least iteration steps.

Nevertheless, some aspects deserve further research: (1) Although the proposed method FSC_LNML has better noise robustness, it takes more time to calculate non-local spatial information. As we can see from Section 4.6, its time complexity is $O(n^5)$, so how to reduce the computational complexity of the non-local information will be the next stage of the task. (2) For the local variance template and non-local variance information, selecting S , l , and σ is still an open problem, how to adaptively calculate these parameters will also be challenging.

CRediT authorship contribution statement

Tongyi Wei: Conceptualization, Methodology, Software, Validation, Formal analysis, Data curation, Investigation, Writing – original draft, Visualization. **Xiaopeng Wang:** Resources, Writing – review & editing, Supervision, Project administration, Funding acquisition. **Xinna Li:** Writing – review & editing. **Shengyang Zhu:** Writing – review & editing.

Declaration of competing interest

The authors declare that they have no known competing financial interests or personal relationships that could have appeared to influence the work reported in this paper.

Acknowledgments

The authors are glad to show appreciation to the anonymous reviewers for their comments and constructive suggestions. This work was supported by the National Natural Science Foundation of China under Grant 61761027.

References

- Ahmed, M.N., Yamany, S.M., Mohamed, N., Farag, A.A., Moriarty, T., 2002. A modified fuzzy c-means algorithm for bias field estimation and segmentation of MRI data. *IEEE Trans. Med. Imaging* 21 (3), 193–199.
- Albu, A., Precup, R.-E., Teban, T.-A., 2019. Results and challenges of artificial neural networks used for decision-making and control in medical applications. *Facta Univ. Ser. Mech. Eng* 17 (3), 285–308.
- Arbelaez, P., Maire, M., Fowlkes, C., Malik, J., 2010. Contour detection and hierarchical image segmentation. *IEEE Trans. Pattern Anal. Mach. Intell* 33 (5), 898–916.
- Bai, X., Chen, Z., Zhang, Y., Liu, Z., Lu, Y., 2015. Infrared ship target segmentation based on spatial information improved FCM. *IEEE Trans. Cybern.* 46 (12), 3259–3271.
- Bai, M., Urtasun, R., 2017. Deep watershed transform for instance segmentation. In: Proceedings of the IEEE Conference on Computer Vision and Pattern Recognition, pp. 5221–5229.
- Borlea, I.-D., Precup, R.-E., Borlea, A.-B., Iercan, D., 2021. A unified form of fuzzy C-means and K-means algorithms and its partitional implementation. *Knowl.-Based Syst.* 214, 106731.
- Buades, A., Coll, B., Morel, J.-M., 2008. Nonlocal image and movie denoising. *Int. J. Comput. Vis* 76 (2), 123–139.
- Cai, W., Chen, S., Zhang, D., 2007. Fast and robust fuzzy c-means clustering algorithms incorporating local information for image segmentation. *Pattern Recognit* 40 (3), 825–838.

- Chatzis, S.P., Varvarigou, T.A., 2008. A fuzzy clustering approach toward hidden Markov random field models for enhanced spatially constrained image segmentation. *IEEE Trans. Fuzzy Syst.* 16 (5), 1351–1361.
- Chen, S., Zhang, D., 2004. Robust image segmentation using FCM with spatial constraints based on new kernel-induced distance measure. *IEEE Trans. Syst. Man. Cybern. Part B* 34 (4), 1907–1916.
- Cocosco, C.A., Kollokian, V., Kwan, R.K.-S., Pike, G.B., Evans, A.C., 1997. Brainweb: Online interface to a 3D MRI simulated brain database. In: NeuroImage. Citeseer.
- Deng, Z., Choi, K.-S., Chung, F.-L., Wang, S., 2010. Enhanced soft subspace clustering integrating within-cluster and between-cluster information. *Pattern Recognit.* 43 (3), 767–781.
- Elazab, A., Wang, C., Jia, F., Wu, J., Li, G., Hu, Q., 2015. Segmentation of brain tissues from magnetic resonance images using adaptively regularized kernel-based fuzzy-means clustering. *Comput. Math. Methods Med.* 2015.
- Feng, C., Li, W., Hu, J., Yu, K., Zhao, D., 2020. BCEFCM_S: Bias correction embedded fuzzy c-means with spatial constraint to segment multiple spectral images with intensity inhomogeneities and noises. *Signal Process.* 168, 107347.
- Gan, G., Wu, J., 2008. A convergence theorem for the fuzzy subspace clustering (FSC) algorithm. *Pattern Recognit.* 41 (6), 1939–1947.
- Gan, G., Wu, J., Yang, Z., 2006. A fuzzy subspace algorithm for clustering high dimensional data. In: International Conference on Advanced Data Mining and Applications. Springer, pp. 271–278.
- Ghamisi, P., Benediktsson, J.A., Ulfarsson, M.O., 2013. Spectral-spatial classification of hyperspectral images based on hidden Markov random fields. *IEEE Trans. Geosci. Remote Sens.* 52 (5), 2565–2574.
- Gong, M., Liang, Y., Shi, J., Ma, W., Ma, J., 2012. Fuzzy c-means clustering with local information and kernel metric for image segmentation. *IEEE Trans. Image Process.* 22 (2), 573–584.
- Guo, F.-F., Wang, X.-X., Shen, J., 2016. Adaptive fuzzy c-means algorithm based on local noise detecting for image segmentation. *IET Image Process.* 10 (4), 272–279.
- Han, Y., Shi, P., 2007. An improved ant colony algorithm for fuzzy clustering in image segmentation. *Neurocomputing* 70 (4–6), 665–671.
- Hasheminejad, M., Vosoughian, M.Z., 2020. AB2C: artificial bee colony for clustering. *Int. J. Artif. Intell.* 18 (2), 51–73.
- Hashemzadeh, M., Oskouei, A.G., Farajzadeh, N., 2019. New fuzzy C-means clustering method based on feature-weight and cluster-weight learning. *Appl. Soft Comput.* 78, 324–345.
- He, Y., Yao, S., Yang, W., Yan, H., Zhang, L., Wen, Z., Zhang, Y., Liu, T., 2021. An extraction method for glacial lakes based on landsat-8 imagery using an improved U-net network. *IEEE J. Sel. Top. Appl. Earth Obs. Remote Sens.* 14, 6544–6558.
- Janmaijaya, M., Shukla, A.K., Muhuri, P.K., Abraham, A., 2021. Industry 4.0: Latent Dirichlet allocation and clustering based theme identification of bibliography. *Eng. Appl. Artif. Intell.* 103, 104280.
- Jiang, F., Ma, L., Broyd, T., Chen, K., 2021. Digital twin and its implementations in the civil engineering sector. *Autom. Constr.* 130, 103838.
- Krinidis, S., Chatzis, V., 2010. A robust fuzzy local information C-means clustering algorithm. *IEEE Trans. Image Process.* 19 (5), 1328–1337.
- Krizhevsky, A., Sutskever, I., Hinton, G.E., 2012. Imagenet classification with deep convolutional neural networks. *Adv. Neural Inf. Process. Syst.* 25, 1097–1105.
- Lei, T., Jia, X., Zhang, Y., He, L., Meng, H., Nandi, A.K., 2018a. Significantly fast and robust fuzzy c-means clustering algorithm based on morphological reconstruction and membership filtering. *IEEE Trans. Fuzzy Syst.* 26 (5), 3027–3041.
- Lei, T., Jia, X., Zhang, Y., Liu, S., Meng, H., Nandi, A.K., 2018b. Superpixel-based fast fuzzy C-means clustering for color image segmentation. *IEEE Trans. Fuzzy Syst.* 27 (9), 1753–1766.
- Li, Shuo, Fevens, T., Krzyzak, A., Song, Li., 2006. Automatic clinical image segmentation using pathological modeling. PCA and SVM. *Eng. Appl. Artif. Intell.* 19 (4), 403–410.
- Liu, J., Lin, M., Chen, W., Zhang, A., Qi, X., Hou, H., 2021. Ecological risks of geological disasters and the patterns of the urban agglomeration in the Fujian Delta region. *Ecol. Indic.* 125, 107475.
- Liu, G., Zhang, Y., Wang, A., 2015a. Incorporating adaptive local information into fuzzy clustering for image segmentation. *IEEE Trans. Image Process.* 24 (11), 3990–4000.
- Liu, G., Zhao, Z., Zhang, Y., 2015b. Image fuzzy clustering based on the region-level Markov random field model. *IEEE Geosci. Remote Sens. Lett.* 12 (8), 1770–1774.
- Long, J., Shelhamer, E., Darrell, T., 2015. Fully convolutional networks for semantic segmentation. In: Proceedings of the IEEE Conference on Computer Vision and Pattern Recognition, pp. 3431–3440.
- Ma, J., Li, S., Qin, H., Hao, A., 2016. Unsupervised multi-class co-segmentation via joint-cut over L_1 -manifold hyper-graph of discriminative image regions. *IEEE Trans. Image Process.* 26 (3), 1216–1230.
- Memon, K.H., Lee, D.-H., 2018. Generalised kernel weighted fuzzy C-means clustering algorithm with local information. *Fuzzy Sets Syst.* 340, 91–108.
- Mishro, P.K., Agrawal, S., Panda, R., Abraham, A., 2020. Novel fuzzy clustering-based bias field correction technique for brain magnetic resonance images. *IET Image Process.* 14 (9), 1929–1936.
- Oskouei, A.G., Hashemzadeh, M., Asheghi, B., Balafar, M.-A., 2021. CGFFCM: Cluster-weight and group-local feature-weight learning in fuzzy C-means clustering algorithm for color image segmentation. *Appl. Soft Comput.* 108005.
- Peizhuang, W., 1983. Pattern recognition with fuzzy objective function algorithms (James C. Bezdek). *SIAM Rev.* 25 (3), 442.
- Pont-Tuset, J., Arbelaez, P., Barron, J.T., Marques, F., Malik, J., 2016. Multiscale combinatorial grouping for image segmentation and object proposal generation. *IEEE Trans. Pattern Anal. Mach. Intell.* 39 (1), 128–140.
- Pozna, C., Precup, R.-E., 2014. Applications of signatures to expert systems modelling. *Acta Polytech. Hungarica* 11 (2), 21–39.
- Shotton, J., Winn, J., Rother, C., Criminisi, A., 2006. Textonboost: Joint appearance, shape and context modeling for multi-class object recognition and segmentation. In: European Conference on Computer Vision. Springer, pp. 1–15.
- Sodjinou, S.G., Mohammadi, V., Mahama, A.T.S., Gouton, P., 2021. A deep semantic segmentation-based algorithm to segment crops and weeds in agronomic color images. *Inf. Process. Agric.*
- Szilagyi, L., Benyo, Z., Szilagyi, S.M., Adam, H.S., 2003. MR brain image segmentation using an enhanced fuzzy c-means algorithm. In: Proceedings of the 25th Annual International Conference of the IEEE Engineering in Medicine and Biology Society (IEEE Cat. No. 03CH37439). IEEE, pp. 724–726.
- Wang, B., Tu, Z., 2012. Affinity learning via self-diffusion for image segmentation and clustering. In: 2012 IEEE Conference on Computer Vision and Pattern Recognition. IEEE, pp. 2312–2319.
- Wang, J., Wang, S., Chung, F., Deng, Z., 2013. Fuzzy partition based soft subspace clustering and its applications in high dimensional data. *Inf. Sci. (Ny)* 246, 133–154.
- Wang, Q., Wang, X., Fang, C., Jiao, J., 2021. Fuzzy image clustering incorporating local and region-level information with median memberships. *Appl. Soft Comput.* 105, 107245.
- Wang, Q., Wang, X., Fang, C., Yang, W., 2020. Robust fuzzy c-means clustering algorithm with adaptive spatial & intensity constraint and membership linking for noise image segmentation. *Appl. Soft Comput.* 92, 106318.
- Wei, D., Wang, Z., Si, L., Tan, C., Lu, X., 2021. An image segmentation method based on a modified local-information weighted intuitionistic fuzzy C-means clustering and gold-panning algorithm. *Eng. Appl. Artif. Intell.* 101, 104209.
- Weng, G., Dong, B., 2021. A new active contour model driven by pre-fitting bias field estimation and clustering technique for image segmentation. *Eng. Appl. Artif. Intell.* 104, 104299.
- Wong, K.W., Gedeon, T., Kóczy, L., 2004. Construction of fuzzy signature from data: an example of SARS pre-clinical diagnosis system. In: 2004 IEEE International Conference on Fuzzy Systems (IEEE Cat. No. 04CH37542). IEEE, pp. 1649–1654.
- Wu, K.-L., Yu, J., Yang, M.-S., 2005. A novel fuzzy clustering algorithm based on a fuzzy scatter matrix with optimality tests. *Pattern Recognit. Lett.* 26 (5), 639–652.
- Xia, G.-S., Hu, J., Hu, F., Shi, B., Bai, X., Zhong, Y., Zhang, L., Lu, X., 2017. AID: A benchmark data set for performance evaluation of aerial scene classification. *IEEE Trans. Geosci. Remote Sens.* 55 (7), 3965–3981.
- Yin, S., Qian, Y., Gong, M., 2017. Unsupervised hierarchical image segmentation through fuzzy entropy maximization. *Pattern Recognit.* 68, 245–259.
- Zaixin, Z., Lizhi, C., Guangquan, C., 2014. Neighbourhood weighted fuzzy c-means clustering algorithm for image segmentation. *IET Image Process.* 8 (3), 150–161.
- Zeng, S., Wang, X., Cui, H., Zheng, C., Feng, D., 2017. A unified collaborative multikernel fuzzy clustering for multiview data. *IEEE Trans. Fuzzy Syst.* 26 (3), 1671–1687.
- Zhang, H., Bruzzone, L., Shi, W., Hao, M., Wang, Y., 2018. Enhanced spatially constrained remotely sensed imagery classification using a fuzzy local double neighborhood information c-means clustering algorithm. *IEEE J. Sel. Top. Appl. Earth Obs. Remote Sens.* 11 (8), 2896–2910.
- Zhang, W., Guo, X., Huang, T., Liu, J., Chen, J., 2019. Kernel-based robust bias-correction fuzzy weighted C-ordered-means clustering algorithm. *Symmetry (Basel)* 11 (6), 753.
- Zhang, H., Wang, Q., Shi, W., Hao, M., 2017. A novel adaptive fuzzy local information c-means clustering algorithm for remotely sensed imagery classification. *IEEE Trans. Geosci. Remote Sens.* 55 (9), 5057–5068.
- Zhao, F., 2013. Fuzzy clustering algorithms with self-tuning non-local spatial information for image segmentation. *Neurocomputing* 106, 115–125.
- Zhao, F., Jiao, L., Liu, H., 2011. Fuzzy c-means clustering with non local spatial information for noisy image segmentation. *Front. Comput. Sci. China* 5 (1), 45–56.
- Zhao, Q., Li, X., Li, Y., Zhao, X., 2017. A fuzzy clustering image segmentation algorithm based on hidden Markov random field models and voronoi tessellation. *Pattern Recognit. Lett.* 85, 49–55.